Bioorganic Chemistry 57 (2014) 171–185

Contents lists available at ScienceDirect

Bioorganic Chemistry

journal homepage: www.elsevier.com/locate/bioorg

Mechanism and inhibition of 1-deoxy-D-xylulose-5-phosphate reductoisomerase

Andrew S. Murkin *, Kathryn A. Manning, Svetlana A. Kholodar

Department of Chemistry, University at Buffalo, Buffalo, NY 14260-3000, United States

ARTICLE INFO

Article history:
Available online 19 June 2014

Keywords:
Reductoisomerase
Enzyme mechanism
Kinetic mechanism
Tuberculosis
Malaria
1-Deoxy-D-xylulose 5-phosphate (DXP)
Fosmidomycin
DXR

ABSTRACT

The non-mevalonate or 2-*C*-methyl-D-erythritol-4-phosphate (MEP) pathway is responsible for generating isoprenoid precursors in plants, protozoa, and bacteria. Because this pathway is absent in humans, its enzymes represent potential targets for the development of herbicides and antibiotics. 1-Deoxy-D-xylulose (DXP) reductoisomerase (DXR) is a particularly attractive target that catalyzes the pathway's first committed step: the sequential isomerization and NADPH-dependent reduction of DXP to MEP. This article provides a comprehensive review of the mechanistic and structural investigations on DXR, including its discovery and validation as a drug target, elucidation of its chemical and kinetic mechanisms, characterization of inhibition by the natural antibiotic fosmidomycin, and identification of structural features that provide the molecular basis for inhibition of and catalysis.

1. DXR and the MEP pathway

The NADPH-dependent conversion of 1-deoxy-D-xylulose 5-phosphate (DXP) to 2-*C*-methyl-D-erythritol 4-phosphate (MEP) is mediated by the enzyme DXP reductoisomerase (DXR). DXR catalyzes this reaction in a single step involving an intramolecular rearrangement followed by a reduction of the resulting aldehyde intermediate. This reaction is part of a series of enzymatic steps in the MEP pathway (non-mevalonate pathway) for the synthesis of isoprenoids, which are essential to all living organisms; thus, DXR is a potential drug target for species that utilize this pathway. In this review the kinetic, mechanistic, and structural properties of DXR are presented, and implications for inhibitor design are discussed.

1.1. Isoprenoid biosynthesis is universally essential

Isoprenoids form the largest class of natural products and are essential metabolites for all living organisms [1]. These compounds are derived from the five-carbon isoprene precursors isopentenyl pyrophosphate (IPP) and dimethylallyl pyrophosphate (DMAPP). The vast number of unique combinations of elongations, rearrangements, cyclizations, and oxidations involving these building blocks accounts for the large diversity in this class of bioorganic products [2]. Isoprenoids play important roles in various biological functions, including prenyl lipids in archaebacteria [3], sterols in eubacteria and eukaryotes [4], light-harvesting pigments such as carotenoids, carriers for electron transport such as ubiquinone and menaquinone, and regulators of growth and development such as steroids, hormones, and cytokinins [5]. Isoprenoids are also effective as herbicides or herbivore repellents [6].

1.2. Discovery of the MEP pathway

The mevalonate pathway (HMG-CoA reductase pathway), which initiates with two molecules of acetyl-CoA and generates IPP in six enzymatic steps, was generally accepted as the only pathway for biosynthesis of isoprenoid precursors (Fig. 1A). In the early 1990s, however, substantial evidence for an alternate route resulted from various ^{13}C-incorporation studies; most notably were the conflicting results using ^{13}C-labeled mevalonate precursors [7–13]. Attempts to incorporate ^{13}C from labeled acetate or

Abbreviations: DMAPP, dimethylallyl pyrophosphate; DX, 1-deoxy-D-xylulose; DXP, 1-deoxy-D-xylulose 5-phosphate; DXR, 1-deoxy-D-xylulose-5-phosphate reductoisomerase; FDP, D-fructose 1,6-diphosphate; IPP, isopentenyl pyrophosphate; ITC, isothermal titration calorimetry; KARI, ketol-acid reductoisomerase; KIE, kinetic isotope effect; MEP, 2-*C*-methyl-D-erythritol 4-phosphate; MEsP, 2-*C*-methyl-D-erythrose 4-phosphate; $NADP^+$, oxidized form of nicotinamide adenine dinucleotide phosphate; NADPH, reduced form of nicotinamide adenine dinucleotide phosphate.

* Corresponding author. Address: 672 Natural Sciences Complex, Buffalo, NY 14260-3000, United States. Fax: +1 (716) 645 6963.
E-mail address: amurkin@buffalo.edu (A.S. Murkin).

http://dx.doi.org/10.1016/j.bioorg.2014.06.001
0045-2068/

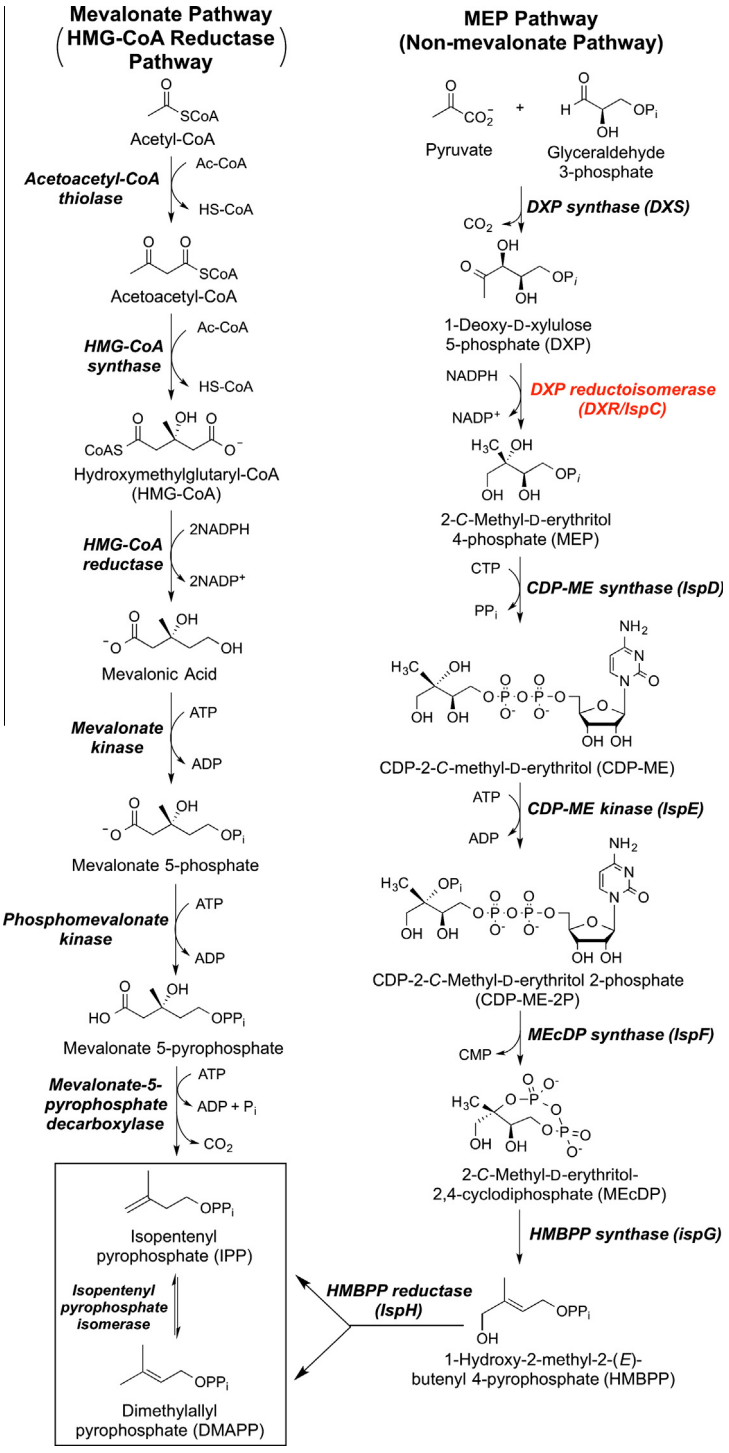

Fig. 1. Biosynthetic schemes of the mevalonate and MEP pathways for IPP and DMAPP production.

mevalonate into isoprenoids in various plant systems [14–16] and into pentalenolactone generated by several species of *Streptomyces* [7,8] proved unsuccessful. Further, experiments utilizing labeled glucose, glycerol, or pyruvate yielded results contradictory to those predicted by the mevalonate pathway, suggesting the existence of an alternative route [11,17–21].

The MEP pathway (non-mevalonate pathway), consisting of seven enzymatic steps leading to IPP and DMAPP, is utilized by many species of bacteria, protozoa, plants, and algae (Fig. 1B). The enzymes in this pathway have been the subject of a recent review [22]. Rohmer and co-workers [20] established that pyruvate and glyceraldehyde 3-phosphate (GAP) are the origins of the isoprenoid carbon atoms in several species of bacteria. It was determined that these two precursors undergo a condensation and decarboxylation to produce DXP as the first intermediate in the pathway [21]. The succeeding reaction catalyzed by DXP reductoisomerase (EC 1.1.1.267; DXR), the subject of this review, converts DXP to the intermediate that lends its name to the

pathway, MEP [23]. Because DXP is also a precursor for vitamin B_1 and B_6 metabolic pathways [24], the DXR-catalyzed reaction is considered the first committed step in this cascade.

1.3. DXR as a potential drug target

Although some species, such as higher plants, have been shown to possess both MVA and MEP pathways [25], species found to utilize this pathway exclusively include pathogens like *Escherichia coli*, *Mycobacterium tuberculosis*, *Mycobacterium leprae*, *Helicobacter pylori*, *Vibrio cholera*, *Bacillus anthracis*, and the malaria causing protozoan *Plasmodium falciparum* [26]. The discovery of this MEP pathway and the determination that it is heterologous from the MVA pathway utilized by humans allows for the potential development of antibacterial and herbicidal drugs with the avoidance of toxicity to humans. This is likely a valid approach for all of the aforementioned disease causing species since the enzymes involved in this pathway have highly conserved sequences [27,28].

The identification of the *E. coli* gene encoding DXR and first successful expression of recombinant protein was reported by Seto and co-workers [23,29]. In this study, *E. coli* mutants were produced and screened for those that were auxotrophic to 2-*C*-methylerythritol (ME), which is the free alcohol analogue known to be used in place of MEP by *E. coli*, and also circumvented the occurrence of poor uptake of the phosphorylated compound. Mutants that could only survive with the addition of ME underwent complementation studies using an *E. coli* genomic library. It was found that the *ispC* gene was responsible for the growth of these mutants, and the resulting enzyme from overexpression of this gene was shown to convert DXP into MEP in a single reaction involving two steps: an isomerization and immediate NADPH dependent reduction, which led to the designation of this enzyme as DXP reductoisomerase [23]. Other DXR knockout studies in *E. coli* [30], *Arabidopsis thaliana* [31], and *Bacillus subtilis* [32], also proved toxic for the respective species, further illustrating the dependence of these organisms on DXR and the MEP pathway. For this reason, DXR was established as a potential target for antimicrobial development.

2. The chemical mechanism of the DXR-catalyzed reaction

2.1. Cofactor usage

DXR requires a divalent metal cation and NADPH as cofactors for catalysis; note that NADPH can more accurately be termed a co-substrate because it is consumed in the reaction.

2.1.1. Metal cofactor

In general, DXR is activated in decreasing order by Mn^{2+}, Co^{2+}, and Mg^{2+} but not by Ba^{2+}, Ca^{2+}, Cu^{2+}, Fe^{2+}, Ni^{2+}, or Zn^{2+} for the enzymes of bacterial origin [29,33–37]. The greater efficacy of DXR bound with Mn^{2+} versus Mg^{2+} is consistent with what is often observed in other cases; it has been argued that the increased flexibility of the metal–ligand bonds exhibited by Mn^{2+} more easily accommodates distortions in coordination geometry at the transition state [38]. The identity of the metal cofactor not only alters its affinity to the enzyme by 2–3 orders of magnitude but also influences the K_m of DXP and NADPH [33–35]. The concentration of divalent metal required for 50% maximal activation, K_{act}, was reported to increase sharply at lower pH values; this was attributed to decreased metal affinity resulting from changes in the protonation state of the chelating carboxylate groups in the active site [33,37]. Interestingly, DXRs from plant sources [39,40] and the parasite *Toxoplasma gondii* [41] exhibited similar degrees of activation by both Mn^{2+} and Mg^{2+} and less or no activation by Co^{2+}, while plant enzymes additionally possessed a capability of metal cofactor promiscuity being able to utilize Cu^{2+}, Fe^{2+}, Ni^{2+} [39], Ca^{2+}, and Zn^{2+} [40].

2.1.2. Dinucleotide cofactor

Preference for NADPH over NADH was reported for the bacterial DXRs from *E. coli* [29], *M. tuberculosis* [33], and *Synechococcus leopoliensis* [42], and for the plant enzymes [39,40]. As reflected in the K_m values measured with *M. tuberculosis* DXR, the primary reason underlying the lower activity with NADH is its two-orders decreased affinity [33]; since k_{cat} is essentially identical for NADPH and NADH [33], the 2′-phosphate group is a binding determinant and is not required for catalysis. Studies with DXR from *Synechocystis* sp. PCC6803 [34], *Zymomonas mobilis* [43], and *E. coli* [29] using a single concentration of NADH showed at least 100-fold reduced activity, but in light of the elevated K_m with *M. tuberculosis* DXR, this may be due to sub-saturation.

2.2. Reaction stereochemistry

Stereochemistry studies using (4*S*)-[4-^{2}H]NADPH with recombinant DXR from *E. coli*, *Synechocystis*, and *M. tuberculosis* concluded that the C-1 pro-*S* hydrogen of MEP originates from the C-3 hydrogen of DXP, while the C-1 pro-*R* hydrogen originates from the C-4 pro-*S* hydride of NADPH upon reduction of the *re* face of MEsP (Fig. 2), making DXR a class B dehydrogenase [44–46]. The same stereochemical conclusion had been reached by Arigoni et al. [47] by soaking plant leaves with 1-deoxy-D-[^{2}H]xylulose (DX), which becomes phosphorylated at C-5 in vivo to produce DXP, and analyzing the 2-*C*-methyl-D-erythritol that results from DXR conversion and dephosphorylation.

2.3. Evidence for carbon-skeleton rearrangement

Even before the *ispC* gene encoding DXR was identified, the occurrence of an intramolecular rearrangement had been revealed by ^{13}C-incorporation experiments. Especially diagnostic were contiguously labeled glucose and DX. Isotope incorporation from [4,5-$^{13}C_2$]glucose into hopanoid and ubiquinone in *Methylobacterium fujisawaense* [20] and from [$^{13}C_6$]glucose into isoprenoids of *Z. mobilis* [21], plastidic isoprenoids of *Scenedesmus obliquus* [12], menaquinones of *Streptomyces aeriouvifer* [13], and dihydromenaquinones of *Corynebacterium ammoniagenes* [17] clearly demonstrated the separation between C-4 and C-5 in glucose in the process of forming labeled IPP and DMAPP (Fig. 3). Branched isoprenoids resulted from ^{13}C incorporation from [2,3,4,5-$^{13}C_4$]DX into phytol and carotenoids in *Catharanthus roseus* [48] and from [2,3-$^{13}C_2$]- and [2,4-$^{13}C_2$]DX into ubiquinone in *E. coli* [49]; in contrast, deuterium incorporation from [1,1-$^2H_2$]MEP resulted in a conserved carbon skeleton in ubiquinone and menaquinone in *E. coli* [18]. These findings demonstrated that isomerization in the MEP pathway occurs during DXP conversion to MEP and that C-4 of DXP is translocated from C-3 to C-2.

2.4. 2-C-methyl-D-erythrose 4-phosphate as a reaction intermediate

The carbon-skeleton rearrangement involved in conversion of DXP to MEP is believed to proceed through the aldehyde intermediate 2-*C*-methyl-D-erythrose 4-phosphate (MEsP), which is subsequently reduced by NADPH (Fig. 4A) [21,48]. This hypothesis was originally based on analogy to ketol-acid reductoisomerase (KARI; EC 1.1.1.86), which catalyzes a similar rearrangement–reduction sequence in the conversion of 2-acetolactate to 2,3-dihydroxy-3-methylbutyrate, a precursor involved in the biosynthesis of branched-chain amino acids (Fig. 4B) [50–52]. The hypothetical intermediate, 3-hydroxy-3-methyl-2-oxobutyrate, has not been

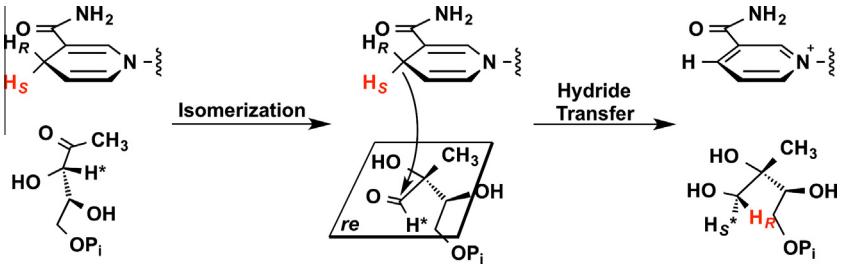

Fig. 2. Stereochemistry of hydride transfer from NADPH to MEsP catalyzed by DXR. The subscripts *R* and *S* indicate the prochirality of the hydrogens.

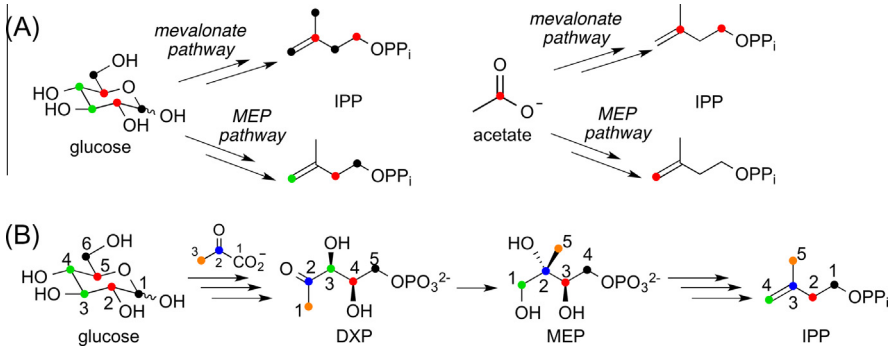

Fig. 3. (A) Labeling patterns in IPP via the mevalonate and MEP pathways observed from incorporation studies using ^{13}C-labeled glucose and acetate. (B) Full carbon labeling pattern expected for DXP, MEP, and IPP from glucose and pyruvate via the MEP pathway.

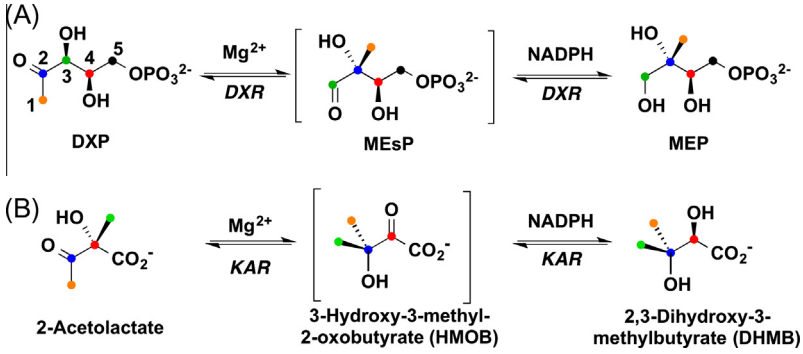

Fig. 4. Reductoisomerase-catalyzed reactions involving sequential carbon-skeleton rearrangement and NADPH-dependent reduction. (A) The DXR-catalyzed conversion of DXP to MEP proceeds through an aldehyde intermediate (MEsP). (B) The KARI-catalyzed conversion of 2-acetolactate to 1,2-dihydroxy-3-methylbutyrate proceeds through a keto intermediate (3-hydroxy-3-methyl-2-oxobutyrate).

directly detected for the KARI-catalyzed reaction [53]; similarly, MEsP was not observed in several DXR studies [23,29]. Attempts by Koppisch et al. [35] to detect MEsP by ^{1}H NMR were unsuccessful, leading the authors to conclude the relative abundance of this intermediate to be <0.2% of the sum of DXP and MEP; the use of sodium borohydride or *N*-methylnitrosohydrazine failed to trap any traces of the aldehyde. Hoeffler et al. [54] noted that the absence of cofactor or the use of dihydro-NADPH, an inactive analogue of NADPH, both failed to induce detectable isomerization of DXP. These observations led to the conclusion that either the rearrangement and reduction steps are coordinated processes such that MEsP is never definitively formed or MEsP is tightly bound to the enzyme prior to NADPH reduction [29,54]; a similar proposal had been made in the case of KARI [53] (see Fig. 4).

Although direct attempts to support MEsP as an intermediate in the DXR-catalyzed reaction yielded negative results, Rohmer and co-workers [54] provided the first compelling supportive evidence by chemically synthesizing MEsP and demonstrating that it is kinetically competent. When incubated with DXR and NADPH in the presence of either Mn^{2+} or Mg^{2+}, MEsP was quantitatively converted to MEP faster than DXP by a factor of 4 or 1.6, respectively. When incubated with the oxidized form of the coenzyme, MEsP was converted to DXP, albeit only to 7%. Similar to observations with KARI and its hypothetical intermediate [55], the K_m for MEsP was found to be greater than that for DXP (294 and 158 μM, respectively, in the presence of Mn^{2+} and Mg^{2+} versus 73 and 97 μM for DXP) [54]. It has been argued that the increased K_m values counter the suggestion of tight binding of the intermediate to these enzymes; however, it is hazardous to equate K_d and K_m, which is true only when substrate dissociation is rapid. If one considers a more general case of the two-step steady-state model (Eq. (1)),

$$E + S \underset{k_{-1}}{\overset{k_1}{\rightleftharpoons}} ES \overset{k_2}{\rightarrow} E + P \quad (1)$$

$K_d = k_{-1}/k_1$ and $K_m = (k_{-1} + k_2)/k_1 = K_d + k_2/k_1$. If reaction of MEsP ($k_2$) is much faster than its dissociation (k_{-1})—in other words, it has a

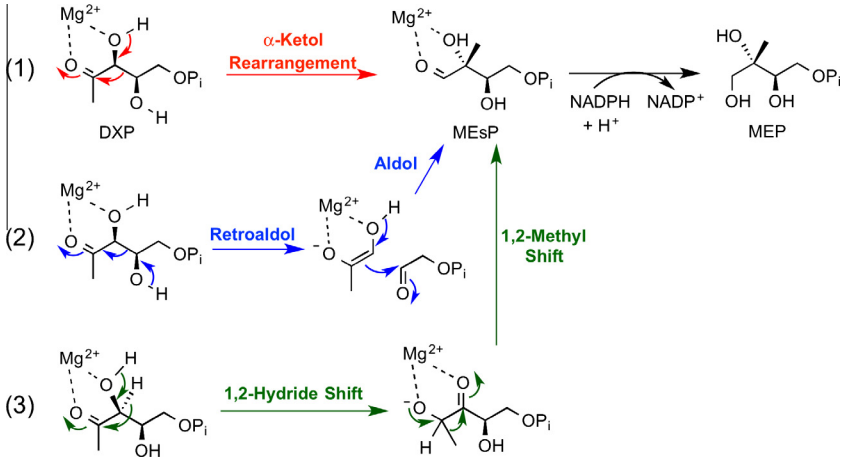

Fig. 5. Three proposed mechanisms for the formation MEsP in the reaction catalyzed by DXR: (1) α-ketol rearrangement, (2) retro-aldolization/aldolization, and (3) sequential 1,2-hydride and 1,2-methyl shifts. Proton-transfer steps have been omitted for clarity. The enediolate intermediate of the retro-aldol/aldol mechanism is arbitrarily depicted in one of two possible tautomers but may also exist as the neutral enediol.

high forward commitment, making it a "sticky" substrate—then its K_m would be dictated by k_2/k_1 [56]; thus, depending on the ratio of k_2 to k_1, MEsP could have a K_m that greatly exceeds its K_d.

2.5. Proposed chemical mechanisms for DXR-catalyzed rearrangement of DXP

Despite the overall similarities between the DXR- and KARI-catalyzed reactions, differences in the amino acid sequences and X-ray crystal structures suggest that the DXR-catalyzed reaction could potentially proceed through a different mechanism [55,57,58]. Thus, three possible mechanisms have been considered for the isomerization of DXP to MEsP: (1) an α-ketol rearrangement, (2) a retro-aldolization/aldolization, and (3) a sequential 1,2-hydride and 1,2-methyl shift (Fig. 5) [43]. The third mechanism was readily eliminated on the basis of the glucose ^{13}C-incorporation studies described above (Section 2.2) [21], in addition to labeled DXP experiments, where [2-^{13}C]- and [3,4,5-$^{13}C_3$]DXP strictly yielded [2-^{13}C]- and [1,3,4-$^{13}C_3$]MEP, respectively [33,59]. Most attention, therefore, has been placed on discriminating between the first mechanism, which is directly analogous to that proposed for KARI (see Section 2.4), and the second mechanism, which parallels ribulose-5-phosphate 4-epimerase [54,60] and bacterial class II aldolases [60,61].

2.5.1. Putative retro-aldol intermediates

The putative intermediates resulting from the retro-aldol cleavage of DXP are glycolaldehyde phosphate and the enediolate of hydroxyacetone. Several studies have attempted to find evidence supporting the generation of these species during turnover [54,62,63]. Incubations of DXR with glycolaldehyde phosphate (1–5 mM), hydroxyacetone (1–50 mM), and NADPH revealed no cofactor oxidation above background when monitoring absorbance at 340 nm [54,62]. Glycolaldehyde [^{32}P]phosphate also did not lead to radioactively labeled DXP or MEP [62]. Moreover, incubation of DXR with [1-^{13}C]DXP and NADPH failed to yield a signal corresponding to [3-^{13}C]hydroxyacetone, indicating this compound is not formed in detectable quantities during the reaction [54].

An extensive label-incorporation study performed by Lauw et al. [63] utilized various combinations of ^{13}C-labeled/unlabeled MEP, glycolaldehyde phosphate, and hydroxyacetone. Similar to earlier studies, the incubation of high concentrations of hydroxyacetone and [$^{13}C_2$]glycolaldehyde yielded no detectable MEP. A mixture of [1-^{13}C]- and [3-^{13}C]MEP and NADP$^+$ with a high concentration of DXR was allowed to reach thermodynamic equilibrium, but no fragment exchange was observed despite thousands of reaction cycles. Likewise, no isotope washout was detected when [1,3,4-$^{13}C_3$]MEP was incubated with unlabeled hydroxyacetone. The results of these studies demonstrate that DXR does not possess aldolase activity and led to the conclusion that either the reaction proceeds via the α-ketol rearrangement mechanism or the putative fragments are tightly confined in the active site during catalysis. With respect to the latter possibility, the authors noted that crystal structures depict DXR's active-site flexible loop (see Section 5.4) to be closed when NADPH and DXP are bound, suggesting that ligand exchange with bulk solvent is precluded. Since the intermediate can access this site when it is added exogenously in place of DXP, the flexible loop is clearly not a rigid barrier, and therefore, the smaller putative intermediates would be expected to exhibit similar access from bulk solvent [63]. The collective negative results from this investigation are consistent with both mechanisms, though fewer assumptions are required for the α-ketol rearrangement [54,63].

An alternative substrate binding mode was offered by Li et al. [64] as an explanation for the inability of DXR to exchange the two putative products of the retro-aldol reaction with bulk solvent. Incubation of DXR with Mg^{2+}, NADPH, and DXP in buffered $H_2{}^{18}O$ resulted in ^{18}O incorporation into C-2 of MEP, which originated as the carbonyl (C-2) in DXP, but not into C-1 or C-3 (see Fig. 3 for atom numbering). According to the retro-aldol/aldol mechanism, each of these three positions exists as a carbonyl, at least transiently, during catalysis, and therefore, could potentially exchange its oxygen with bulk solvent. The absence of isotope exchange was considered to be indicative of protection due to coordination of the carbonyl oxygen to the divalent metal, while the occurrence of exchange was deemed the result of a lack of coordination. Thus, the authors argued that, in conjunction with previous studies that suggest DXP's C-3 and C-4 hydroxyl groups are essential for catalysis (see Section 2.5.2) [54,65], DXP binds to the divalent metal via a C3–C4 binding mode (Fig. 6) rather than the generally accepted C2–C3 mode [26,37,66,67]. It was suggested that the inability of DXR to reunite the two putative intermediates when added exogenously was due to the infrequent termolecular process that would need to occur in order to form a reactive complex. The absence of the reverse process—that is, aldolase-like release of the enediolate and glycolaldehyde intermediates—was reasoned to be the result of tight binding of these fragments via the C3–C4 mode. The tight metal coordination suggested to accom-

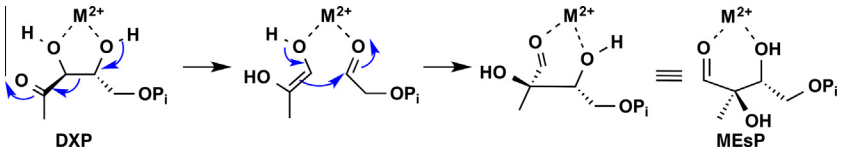

Fig. 6. Hypothetical alternative binding mode for DXP featuring coordination to the active-site divalent metal (M^{2+}) via O-3 and O-4.

pany this binding mode additionally accounts for the kinetic competence of exogenous MEsP and explains why it may not be readily released from the active site during catalysis. Evidence for the C3–C4 binding mode rests on interpretation of the ^{18}O exchange experiment. The results could alternatively be interpreted as supporting the C2–C3 binding mode if one considers that as a Lewis acid, the divalent metal would increase the electrophilicity of the coordinated carbonyl and therefore promote hydration. Further, the absence of exchange at the other positions could be the result of the transiency of the intermediates; exchange into MEP's oxygen atoms at C-1 (via MEsP) and C-3 (via glycolaldehyde phosphate) requires the rate of on-enzyme hydration to rival the rates of hydride transfer and aldolization (either back to DXP or forward to MEsP), respectively.

2.5.2. DXP analogues

Among the first kinetic evidence supporting the retro-aldol/aldol pathway (or more precisely, failing to exclude it) was the absence of activity upon removal or modification of DXP's C-4 hydroxyl group. This moiety is necessary for the retro-aldol/aldol process but would not play a direct role in the α-ketol rearrangement. 1,4-Dideoxy-D-xylulose 5-phosphate failed to serve as a substrate for *E. coli* [54] and *Synechocystis* sp. [68] DXR, though it displayed inhibition (K_i = 120 μM and 30 μM, respectively) comparable to DXP's K_m (73 μM and 170 μM, respectively), indicating that the C-4 hydroxyl is required for turnover but not binding. The C-4 epimer of DXP (i.e., 1-deoxy-L-ribulose 5-phosphate) similarly failed to be converted by DXR but acted as a competitive inhibitor (K_i = 180 μM) [68]. Substitution of a fluorine for the C-4 hydroxyl group of DXP again resulted in a lack of turnover but inhibited (K_i = 770 μM) *E. coli* DXR [65]. Because these inhibitors were all reasonably good ligands but could not be processed by the enzyme, the retro-aldol/aldol mechanism appeared favorable.

DXP analogues fluorinated at C-1 were also studied in an attempt to distinguish between the two mechanisms through inductive electronic effects in formation of the transition state during the rate-limiting step in the reaction. The groups of Liu and Poulter independently synthesized 1-fluoro-DXP and demonstrated its competence as a substrate for *E. coli* DXR [62,65]. Liu and co-workers [65] argued that the electron-withdrawing nature of the fluorine substituent would render the carbonyl more electronegative and thereby accelerate a 1,2-migration. Although the authors acknowledged that the fluorine would also promote a retro-aldol cleavage through stabilization of the incipient enediolate, they noted that it may slow the subsequent aldol step. 1-Fluoro-DXP was found to be a slightly poorer substrate than DXP, with a similar K_m and fourfold lower k_{cat}, prompting the authors to favor the retro-aldol/aldol mechanism [65]. Fox and Poulter offered different reasoning. They asserted that the α-ketol rearrangement requires the carbonyl oxygen either to be protonated or to coordinate to the divalent metal to facilitate cleavage of the carbon–carbon bond (Fig. 7). They also noted that the basicity of a ketone carbonyl is reduced by each addition of an α fluorine [69]; thus, a weakening in the ability of the ketone to complex with the metal was expected. Because formation of the oxacarbenium ion undergoing rearrangement is typically much slower than the sigmatropic rearrangement itself, the α fluorine was anticipated to decelerate such a process, not accelerate it, as had been suggested previously [65]. Conversely, an α fluorine would facilitate the retro-aldol reaction by stabilizing the developing enediolate, as was also argued by Wong et al. [65]; this step was proposed to be rate determining in the rearrangement. In contrast to the results by Liu and co-workers, 1-fluoro-DXP was reported to be as good of a substrate as DXP, with similar k_{cat} (37 versus 21 s^{-1}) and single-turnover rate (k_{max} = 61 s^{-1} for both). This result was taken as support for the retro-aldol/aldol rearrangement, provided that the isomerization step was at least partially rate limiting in the overall reaction (see Section 2.5.3).

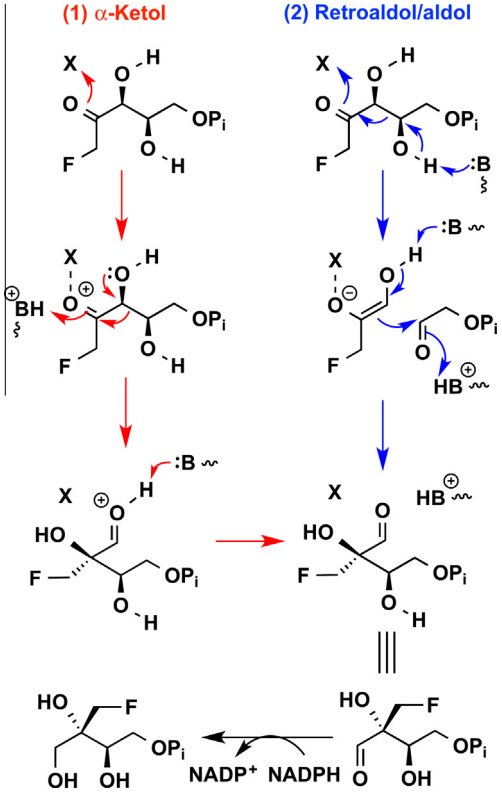

Fig. 7. DXR catalysis of 1-fluoro-DXP through (1) the α-ketol rearrangement and (2) the retro-aldol/aldol mechanisms. Adapted from Fox and Poulter [62].

2.5.3. Kinetic isotope effects for isomerization

Although the substrate analogue studies are consistent with the retro-aldol/aldol mechanism, functional group manipulations often alter unintended parameters such as sterics and electronics, and the results can be confounding. Kinetic isotope effects (KIEs) provide an attractive alternative, as they introduce a kinetically accessible perturbation in the substrate without changing its structure or electronics.

To better discern between the two possible rearrangement mechanisms, α-secondary KIEs were measured for [3-^{2}H]- and [4-^{2}H]DXP. In the case of the α-ketol rearrangement, C-3 undergoes rehybridization from sp^3 to sp^2 while C-4 remains sp^3

hybridized. Because the C–H bond is looser when sp^2 hybridized (due to its predominant lower-frequency out-of-plane bend), this situation is expected to yield normal (i.e., KIE > 1) and unit KIE values, respectively, at C-3 and C-4. In contrast, during the retro-aldol cleavage, both C-3 and C-4 undergo rehybridization from sp^3 to sp^2 and are expected to yield normal KIEs [70]. Thus, the magnitude of these KIEs can differentiate the two mechanisms, provided that isomerization is at least partially rate limiting, which was established for *E. coli* [62] and *M. tuberculosis* [33] DXRs (see Section 3.2).

An initial attempt to measure the 3- and 4-^{2}H KIEs on k_{cat} and k_{cat}/K_m (symbolized ^DV and $^D(V/K)$, respectively) for *E. coli* DXR was undertaken by Wong and Cox [71]. The unlabeled and two deuterated DXPs were synthesized by three different routes, and their steady-state kinetic parameters were measured individually using a spectrophotometric assay. Calculating the KIEs as the quotients of the rate constants, Wong and Cox reported inverse $^D(V/K)$ of 0.92 and 0.86, respectively, for [3-^{2}H]- and [4-^{2}H]DXP and very large, inverse ^DV of 0.56 and 0.62, respectively. They reasoned that this was evidence for the retro-aldol/aldol pathway whereby the aldol step, involving a rehybridization at both positions from sp^2 to sp^3, is rate limiting. However, their measured ^DV values exceed the range of secondary deuterium KIEs. Munos et al. [70] suggested that the erroneous KIEs could be attributable to the variable ee values (74–84%) of their chemically synthesized DXPs [72]; if their unlabeled DXP had a lower ee than the deuterated DXP isotopologues, then inverse KIEs would artificially result. To avoid such factors that plague KIE determinations by direct comparison of rates, Munos et al. [70] repeated the measurements using equilibrium perturbation, in which the light and heavy isotopologues react simultaneously, and any inhibitors present would affect the forward and reverse directions equally [70,73]. The corresponding secondary KIEs were both normal—1.04 for [3-^{2}H]DXP and 1.11 for [4-^{2}H]DXP—strongly supporting the retro-aldol/aldol mechanism. The slightly lower magnitude of these ^{2}H KIEs compared to muscle aldolase, which employs a similar mechanism, was suggested to be reflective of a partially rate-limiting rearrangement or an early transition state. Further, it was suggested that the 4-^{2}H KIE is larger than the 3-^{2}H KIE because C-4 has more s-character than C-3 in the transition state such that the negative charge at C-3 has not yet delocalized completely onto the carbonyl at C-2 in the transition state.

Complementary to the deuterium KIE determinations, ^{13}C KIEs were determined by Manning et al. [74] for *M. tuberculosis* DXR using a method based on 2D [^{13}C,^{1}H]-HSQC NMR. This highly precise technique employs an internal competition for measurement of KIEs, in which light (^{12}C) and heavy (^{13}C) substrates are reacted simultaneously in the same mixture with the enzyme. As the reaction proceeds under the influence of a KIE, the $^{13}C/^{12}C$ ratio (R) of the remaining substrate is observed to increase due to the faster consumption of the light isotopologue. The KIE is obtained by plotting R as a function of the fraction of conversion (F) and fitting the data to Eq. (2),

$$R/R_0 = (1 - F)^{1/KIE-1} \quad (2)$$

where R_0 is the initial value of R. Using this method, Manning et al. [74] measured 2-, 3-, and 4-^{13}C KIEs of 1.0031, 1.0303, and 1.0148, respectively. Whereas the latter two are large enough to be primary KIEs (i.e., involving σ bond formation/cleavage), the smaller 2-^{13}C is not. Because the alkyl migration of the α-ketol rearrangement requires primary ^{13}C KIEs at all three positions, this mechanism was excluded. Further, because the retro-aldol step involves cleavage of the C3–C4 bond with minimal change at C-2, these KIEs indicate that this step cleanly limits the retro-aldol/aldol sequence.

3. Kinetic mechanism

Steady-state kinetic parameters have been reported for DXR from various organisms of prokaryotic and eukaryotic origins (Table 2). The values of many of these parameters spread over a few orders of magnitude due to several variables including the source organism, engineered features of the enzymes, and assay conditions (in particular temperature and the metal cofactor). Due to its high cellular concentration, Mg^{2+} is often considered to be the physiologically relevant cofactor used by DXR [33–35]; accordingly, it was employed in determinations of most of the parameters in Table 2.

3.1. Substrate/product binding order and equilibrium constant

Detailed investigations of the kinetic mechanism have been performed for *E. coli* [35,65] and *M. tuberculosis* [33,75] DXRs. Upon inspection of the patterns of dead-end inhibition by the DXP analogue fosmidomycin and the NADPH analogue 1,4,5,6-tetrahydro-NADP (also referred to as dihydro-NADPH or $NADPH_3$), a steady-state ordered mechanism with NADPH adding before DXP was concluded for the *E. coli* enzyme [35]. Consistent with this model, the observed non-competitive patterns of inhibition by fluorinated DXP mimics versus DXP and apparent substrate inhibition by DXP led to the conclusion that MEP dissociates before $NADP^+$ and that DXP can bind nonproductively to the E·$NADP^+$ complex (Fig. 8A) [65]. Computer simulations using this mechanism (Fig. 8A, black) were consistent with data acquired in an equilibrium perturbation experiment (see Section 2.5.3), which was used to determine deuterium KIEs for *E. coli* DXR [70]. In the case of the *M. tuberculosis* enzyme, product inhibition and KIE studies by Argyrou and Blanchard [33] and transient kinetic investigations by Liu and Murkin [75] established a steady-state mechanism with

Table 1
Kinetic isotope effects for DXR.

Organism	Label position	Predicted KIE[a]		Expt. KIE	Ref.
		α-Ketol rearrangement	Retro-aldol/aldol rearrangement		
Escherichia coli	DXP 3-^{2}H	α-2° (1.0–1.5)	α-2° (1.0–1.5)	1.04[b]	[70]
	DXP 4-^{2}H	No KIE (~1)	α-2° (1.0–1.5)	1.11[b]	
	NADPH 4-^{2}H	1° (2–7)		1.02[c]	[62]
Mycobacterium tuberculosis	DXP 2-^{13}C	1° (1.01–1.07)	α-2° (~1)	1.0031[d]	[74]
	DXP 3-^{13}C	1° (1.01–1.07)	1° (1.01–1.07)	1.0303[d]	
	DXP 4-^{13}C	1° (1.01–1.07)	1° (1.01–1.07)	1.0148[d]	
	NADPH 4-^{2}H	1° (2–7)		2.2[e]	[33,110]

[a] Assuming the following are the rate-limiting steps: isomerization for α-ketol, retro-aldol step for retro-aldol/aldol, and hydride transfer. If more than one step is partially rate limiting, KIEs would be expected to be toward the lower end of the predicted range.
[b] Calculated by numerical simulation to equilibrium perturbation data.
[c] Measured by direct comparison of single-turnover kinetics data.
[d] Measured by competition by 2D [^{1}H,^{13}C]-HSQC NMR.
[e] Measured by direct comparison of steady-state kinetics data.

Table 2
Comparison of kinetic parameters of DXRs from various organisms.[a]

Organism	Protein construct	T (°C)	k_{cat} (s^{-1})	$k_{cat}/K_{m,DXP}$ ($M^{-1}\,s^{-1}$)	K_m (μM)		$K_{act,Mg}$ (μM)[b]	Ref.
					DXP	NADPH		
Bacteria								
Escherichia coli	Native	37	116	$1.0 \cdot 10^6$	115	0.5	ND[c]	[35]
	Native	37	12	$4.0 \cdot 10^5$	30	ND[c]	ND[c]	[116]
	His-tagged	37	7[d]	$1 \cdot 10^5$ [d]	73	ND[c]	ND[c]	[54]
	His-tagged	37	0.2	$2 \cdot 10^3$	99	18	ND[c]	[36]
Mycobacterium tuberculosis	Native	25	2.1	$5 \cdot 10^4$	42	5.0	1200	[33]
	His-tagged	25	5.3	$4.6 \cdot 10^4$	115	9.8	ND[c]	[75]
Synechocystis sp.	Native	37	5.0	$3.7 \cdot 10^4$	134	5.0	2370	[34]
	His-tagged	37	7.0	$4.1 \cdot 10^4$	170	4.6	ND[c]	
Zymomonas mobilis	His-tagged	40	14[d]	$4.7 \cdot 10^4$ [d]	300	5	ND[c]	[43][e]
Francisella tularensis	His-tagged	22	2.0[f]	$1.9 \cdot 10^4$	104	13.3	ND[c]	[84]
Streptomyces coelicolor	Native	25	19.2	$1.0 \cdot 10^5$	190	190	ND[c]	[117]
Thermotoga maritima	His-tagged	50	0.29	$7.5 \cdot 10^3$	40	2.8	ND[c]	[85]
Protozoa								
Plasmodium falciparum HB3	His-tagged	30	ND[c]	ND[c]	106	ND[c]	ND[c]	[86][e]
Toxoplasma gondii	His-tagged	30	ND[c]	ND[c]	26	ND[c]	ND[c]	[41]
Plantae								
Arabidopsis thaliana	His-tagged	37	4.4	$3.3 \cdot 10^4$	132	30	1000	[39]
Coleus forskohlii	His-tagged	37	0.25[d]	$1.7 \cdot 10^3$ [e]	147.2	82.5	ND[c]	[40][e]

[a] Measured in the presence of Mg^{2+}, unless stated otherwise.
[b] Concentration of the metal ion required for half-maximal activity at saturating substrate concentrations.
[c] ND = not determined.
[d] Calculated from the reported specific activity.
[e] In the presence of $MnCl_2$.
[f] A k_{cat} of 1.3 s^{-1} was reported when NADPH was the variable substrate and the enzyme was 79% saturated with DXP.

random binding of NADPH and DXP but ordered release of the products, $NADP^+$ followed by MEP (Fig. 10B). Additionally, NADPH was demonstrated to be a "sticky" substrate, tending to proceed through the reaction in preference to dissociating from the Michaelis complex [33]; this behavior is reflected in a fourfold lower K_m relative to its K_d [75]. Due to the much lower K_m of NADPH versus DXP, the operational pathway of the reaction favors binding of NADPH prior to DXP (Fig. 10B, blue), except at low concentrations of the cofactor [75]. The final step, release of MEP, is partitioned into one of two alternative pathways: direct dissociation (Fig. 10B, green), which is the minor pathway when NADPH is saturating, and dissociation from the nonproductive E·NADPH·MEP complex (Fig. 10B, red), which is the predominant pathway. In contrast to the proposed *E. coli* DXR mechanism, no appreciable binding of DXP or MEP to the E·$NADP^+$ complex (Fig. 10B, gray) was observed for *M. tuberculosis* DXR, suggesting E·$NADP^+$ is an effectively dead-end complex [75].

The reversibility of the reaction (i.e., conversion of MEP to DXP) has been shown for *E. coli* and *M. tuberculosis* DXRs [33,35,54,75]. The external equilibrium constant, K'_{eq}, for the formation of MEP at pH 7.5 was estimated to by several groups using different methods to be in the range of 27–69 [33,35,54]. An internal equilibrium constant of 22 was calculated for *M. tuberculosis* DXR using the ratio of forward and reverse microscopic rate constants obtained from kinetic simulation [75]. These findings indicate that the physiological reaction direction is favored both on and off the enzyme, consistent with the "descending staircase" free energy model described by Benner and co-workers [76] in which optimal enzyme catalysis is achieved when each catalytic step is energetically favorable.

3.2. Rate-limiting steps

KIE measurements [33,74] and transient kinetic analysis [75] for *M. tuberculosis* DXR indicate that k_{cat}/K_m is partially limited by chemistry, while k_{cat} is additionally limited by release of the second product MEP. The slow release of MEP was associated with a burst of NADPH oxidation nearly stoichiometric with the *M. tuberculosis* DXR concentration under pre-steady-state conditions [75]; interestingly, this behavior was not observed for the *E. coli* enzyme [62], suggesting that the reaction free energy profiles for these orthologues may differ.

The relative barrier for the reduction step has been examined for *E. coli* and *M. tuberculosis* DXRs by determination of the primary deuterium KIE for hydride transfer. Argyrou and Blanchard [33] reported moderate values of $^{D}V = 1.3$ and $^{D}(V/K_{DXP}) = 2.2$ for *M. tuberculosis* DXR using (4*S*)-[4-^{2}H]NADPH, indicating a partially rate-limiting reduction step. The suppressed KIE on k_{cat} (V_{max}) was explained by the fact that this rate constant and not k_{cat}/K_m includes slow release of the second product, MEP [75]. Interestingly, the identity of the metal cofactor was found to influence the magnitudes of these KIEs and correspondingly the nature of rate-limiting steps of the reaction. Specifically, because both ^{D}V and $^{D}(V/K_{DXP})$ were significantly higher with Mn^{2+} than with Mg^{2+} or Co^{2+}, at least one step other than hydride transfer (e.g., isomerization, enzyme conformational change(s), or product release) was suggested to be slower for the latter two metal ions [33]. Fox and Poulter [62] followed this study by demonstrating the absence of a KIE with *E. coli* DXR under single-turnover conditions. In this case, excess enzyme relative to NADPH/NADPD was employed to restrict the observed signal change to steps up to and including hydride transfer during the first turnover. The unit KIE therefore suggests that a step prior to reduction is rate limiting for *E. coli* DXR. Curiously, hydride transfer could be rendered partially rate limiting by using 1-fluoro-DXP as the substrate, resulting in a KIE of 1.34 [62]. This change in rate-determining step indicates that the introduction of fluorine either decelerates hydride transfer or accelerates a previous step, such as rearrangement. The authors favored the latter explanation, taking it as evidence for the retro-aldol/aldol mechanism, in which the fluorine would be predicted to stabilize the enediolate formed during the retro-aldol step (recall Section 2.5.2).

If the rearrangement step is fully rate limiting in the reaction catalyzed by *E. coli* DXR, as suggested by the above primary KIE

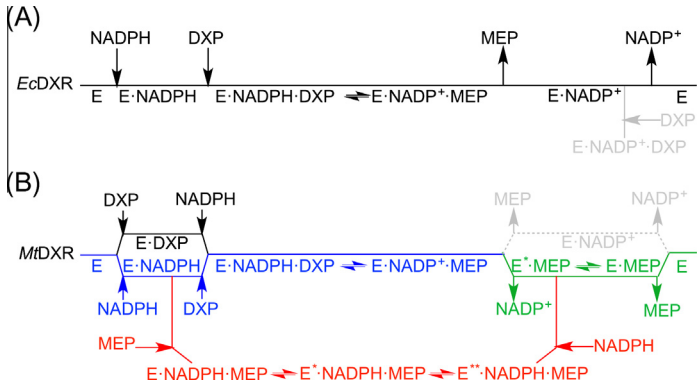

Fig. 8. (A) Proposed kinetic mechanism of *E. coli* DXR (*Ec*DXR). (B) Kinetic mechanism of *M. tuberculosis* DXR (*Mt*DXR).

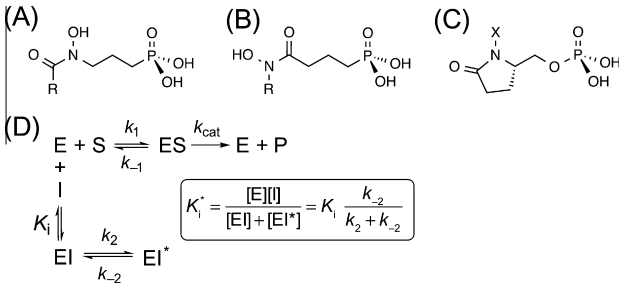

Fig. 9. Fosmidomycin, analogues, and slow tight-binding inhibition mechanism. (A) Fosmidomycin (R = H) and FR-900098 (R = Me). (B) Reverse hydroxamic analogues (R = H or Me) from Kuntz et al. [81]. (C) Cyclic carbamate analogues (X = H or OH) from Mercklé et al. [83]. (D) Two-step mechanism for slow tight binding of fosmidomycin to DXR.

studies, one would expect the "half reaction" consisting of reduction of MEsP by NADPH to proceed much faster; however, as described in Section 2.4, exogenous MEsP was converted to MEP by *E. coli* DXR only 1.6-fold faster than DXP in the presence of Mg^{2+} [54]. Although this result appears at odds, it can be explained by the existence of a slow conformational change associated with MEsP binding, a step that is foreign (and detrimental) to the physiological reaction with DXP. Transient kinetics and KIE experiments on the "half reaction" may provide a resolution.

The rate limitation of the isomerization step was assessed by KIEs using labeled DXP, discussed earlier (Section 2.5.3). The moderate primary 3- and 4-^{13}C KIEs and small secondary 2-^{13}C KIE measured by Manning et al. [74] for *M. tuberculosis* DXR indicate that rearrangement is partially rate limiting overall and more specifically that the two-step isomerization is cleanly limited by the retro-aldolization. The α-secondary 3- and 4-^{2}H KIEs reported by Munos et al. [70] for *E. coli* DXR similarly indicate that isomerization contributes to rate limitation with this orthologue. At 1.04 and 1.11, respectively, these KIEs are much smaller than expected for complete rehybridization from sp^3 to sp^2 at C-3 and C-4, indicating that this process has an early (i.e., DXP-like) transition state or it is only partially rate limiting. Additional KIE experiments are necessary to distinguish between these possibilities.

4. Inhibition by fosmidomycin

To date, the design of inhibitors targeting DXR has been almost entirely centered on structural alterations of the parent compound fosmidomycin (Fig. 9A), a natural antibiotic isolated from the actinobacterium *Streptomyces lavendulae* [77]. Several reviews provide comprehensive background on the design, synthesis, and biological evaluation of fosmidomycin analogues [26,78,79]. Here, we focus on the kinetics and thermodynamics of interactions between DXR and fosmidomycin.

4.1. Kinetics of fosmidomycin inhibition

The kinetics of inhibition by fosmidomycin has been characterized to different extents for DXRs of various species (Table 3). Fosmidomycin mimics DXP [66], serving as a competitive inhibitor against *Z. mobilis* [43] and *A. thaliana* [39] DXRs with K_i values of 600 and 85 nM, respectively. In apparent contrast, initial studies on the inhibition of the *E. coli* [23] and *Synechocyctis* [80] enzymes reported mixed (non-competitive) inhibition versus DXP. More detailed investigations of the pre-steady-state phase of inhibition revealed that fosmidomycin is actually a slow-onset, tight-binding inhibitor often described as following a two-step binding mechanism (Fig. 9D) [35,80,81]. Initial weaker binding to the same enzyme form that binds DXP determines the competitive inhibition pattern and is characterized by the constant K_i, while an overall binding process leading to the tighter complex EI* gives rise to a non-competitive profile with an inhibition constant K_i^*. The ratio K_i/K_i^* indicates the increase in inhibition resulting from the slow, thermodynamically favorable process, often considered a conformational change that leads to stronger enzyme–inhibitor interactions [82]; this ratio is dictated by the relative magnitudes of the rate constants for formation (k_2) and breakdown (k_{-2}) of EI* (Fig. 9D, inset). The values of K_i/K_i^* vary from 4 to 10 for *E. coli* DXR [35,81,83] up to 225 for *Synechocystis* DXR [80], indicating that the favorability of the purported equilibrium depends on the enzyme's source. Based on these observations, the slow, tight-binding behavior of fosmidomycin was assumed for DXRs from *Francisella tularensis* [84], *Thermotoga maritima* [85], *P. falciparum* [86], and *T. gondii* [41]; by pre-incubating these enzymes with the inhibitor for 5–10 min prior to initiation of the reaction with DXP, the slow-onset phase was avoided, and therefore, the observed inhibition constants in these cases represent K_i^* (Table 3). Interestingly, fosmidomycin analogues with a reversed hydroxamic moiety (Fig. 9B) also exhibit slow, tight-binding behavior [81], while phosphonate derivatives containing a conformationally locked carbamate (Fig. 9C) do not [83].

4.2. Fosmidomycin binding mode

Binding of fosmidomycin in the active site of DXR is determined by two major interactions: (1) chelation by the oxygens of the hydroxamic moiety to the bound metal cofactor (Mg^{2+} or Mn^{2+}) and (2) electrostatic/H-bond interactions between the active site and the phosphonate group. The identity of the metal cation, Mg^{2+} or Mn^{2+}, does not influence the affinity of fosmidomycin to

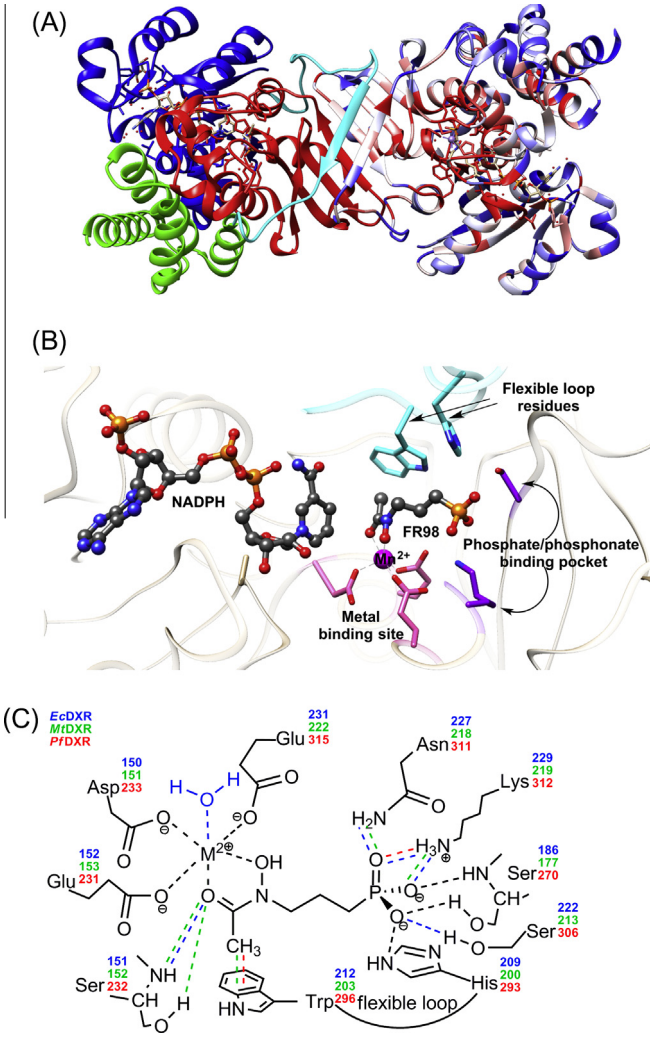

Fig. 10. X-ray crystal structures of DXR complexes. (A) The overall structure of *Mt*DXR complex with Mn^{2+}, FR-900098 and NADPH (PDB 4A03 [104]). The domain structure is illustrated on Chain A (Right): N-terminal domain (blue), central catalytic domain (red), connecting region (cyan) and C-terminal domain (green). Sequence conservation of DXRs from organisms listed in the Tables 1 and 2 is shown on Chain B (Left) according to the percentage of sequences sharing the same residue: red = 100%; white = 50%; blue = 20%. (B) The active site of *M. tuberculosis* DXR bound with Mn^{2+}, FR-900098 (FR98), and NADPH (PDB 4A03 [104]). Key residues and binding pockets are outlined. (C) Schematic illustration of interactions between FR-900098 and active site residues of DXR. Conserved (black) and unique (colored) interactions and residues for *E. coli* (blue), *M. tuberculosis* (green), and *P. falciparum* (red). Images in (A and B) were created with UCSF Chimera [121].

DXR, as determined by inhibition (Table 3) and isothermal titration calorimetry (ITC) [86]. The absence of metal cofactor led to a failure to observe binding of fosmidomycin to the enzyme in ITC experiments, suggesting that chelation is a binding requisite; however, *E. coli* DXR was shown to co-crystallize with NADPH and a high concentration (10 mM) of fosmidomycin in the absence of any divalent metal [37]. Moreover, non-chelating phosphonates were reported to bind and moderately (in the micromolar range) inhibit the enzyme [86–88]. Thus, metal chelation by fosmidomycin in the active site of DXR is important for high affinity but not an essential interaction. On the contrary, substitution of the phosphonate group of fosmidomycin with an aryl halide or heterocyclic group [87], uncharged sulfone or sulfonamide groups, and singly-charged sulfamate, carboxylate, or phosphonate monoesters [80,89,90] impaired the inhibitory activity of corresponding analogues by several orders of the magnitude in comparison to fosmidomycin. These findings emphasize the importance of the phosphodianion anchoring group of fosmidomycin and its derivatives. Additionally, structural [91] and kinetic [92] investigations have suggested that this moiety is an allosteric effector, triggering closure of a flexible loop over the active site of DXR (see Section 5.4).

4.3. Thermodynamics of fosmidomycin binding

While the kinetics of fosmidomycin interactions with DXR have been a subject of many investigations for almost two decades, the thermodynamic aspect of these interactions came into focus only recently. Cai and co-workers [86] reported a thermodynamic investigation of fosmidomycin binding to DXRs from *E. coli*, *M. tuberculosis*, and *P. falciparum*. The affinity of fosmidomycin to *E. coli* and *P. falciparum* DXRs is essentially the same and an order of magnitude higher than that to the *M. tuberculosis* enzyme (Table 2). In contrast, the thermodynamic signatures of fosmidomycin's interaction with *P. falciparum* and *M. tuberculosis* DXRs are similar, featuring exothermic binding driven equally by enthalpic and entropic components, while binding to *E. coli* DXR is endothermic and strongly entropy-driven. This behavior has been rationalized by a difference in degree of hydration of the unliganded metal-binding site in which the *E. coli* enzyme is significantly more hydrated.

4.4. Pharmacokinetics

With the exception of sulfur-containing isosteres [93], the potency of fosmidomycin and its acetyl analogue FR-9800098 (Fig. 9A) has never been dramatically outcompeted despite significant efforts in inhibitor design. These inhibitors are effective against the growth of malaria-causing *P. falciparum* in vitro and in vivo (Table 3) [94], and fosmidomycin has shown clinical success in clearing malarial infections in combination with clindamycin [95]. Unfortunately, both compounds have poor bioavailability and do not exhibit antitubercular activity [79,96]. Uptake studies have confirmed that unlike with Gram-negative bacteria, fosmidomycin does not accumulate intracellularly in *M. tuberculosis* [97]. One of the reasons underlying the poor pharmacokinetics of fosmidomycin is its polar, anionic character, hindering transport through the lipid-rich mycobacterial cell wall or the several membranes leading to the plasmodial apicoplast, the organelle containing the enzyme. Three inhibitor-design strategies aimed to increase the inhibitor's hydrophobicity include (1) esterified prodrugs that undergo conversion to the intact form of fosmidomycin inside the cell [79,98], (2) introduction of lipophilic moieties onto the backbone of fosmidomycin [87,98,99], and (3) replacement of the phosphonate dianion moiety by lipophilic groups [87,100]. Esterification has shown to be the most successful of these approaches to date in improving antimicrobial efficacy [79,98].

5. Structural studies

5.1. Overall structure of DXR

Structures of DXR and its complexes have been investigated by X-ray crystallography, solution NMR [101,102], and molecular dynamics [103]. These structures reveal that all known DXRs exist as homodimers (each subunit molecular weight is 39–45 kDa) with similar overall 3D arrangement [67,91]. The crystal structures to date reveal an asymmetric homodimer comprised of an N-terminal NADPH-binding domain (a member of the classical Rossmann-type dinucleotide-binding domains), catalytic domain, connecting region, and C-terminal domain (Fig. 10A, chain A). The integrity of the dimer in maintained upon formation of multiple salt-bridges

Table 3
Inhibition of DXRs from various organisms by fosmidomycin.

Organism[a]	Ref.	Divalent metal	Inhibition mode[b]	T (°C)	K_i (nM)	Biological activity[c]
Bacteria						
Escherichia coli (native)	[35]	Mg^{2+}	Slow tight-binding	37	K_i = 215 K_i^* = 21	ND[d]
Escherichia coli (His-tagged)	[23]	Mn^{2+}	Mixed	37	38	3.13 μg/mL
	[83]	Mn^{2+}	Slow tight-binding	37	K_i = 27.2 K_i^* = 4.1	ND[d]
	[81]	Mg^{2+}	Slow tight-binding	37	K_i = 40 K_i^* = 10	10 μM
	[88]	Mg^{2+}	STB assumed[e]	30	27	ND[d]
Mycobacterium tuberculosis (native)	[79]	Mg^{2+}	ND[d]	30	ND	>500 μg/mL
Mycobacterium tuberculosis (His-tagged)	[96]	Mg^{2+}	ND[d]	30	150[f]	ND[d]
	[88]	Mg^{2+}	STB assumed[e]	30	140	ND[d]
	[110]	Mg^{2+}	Slow tight-binding	25	93	ND[d]
Synechocystis sp.	[80]	Mn^{2+}	Mixed Slow tight-binding	37	57 (mixed) K_i = 900 K_i^* = 4	ND[d]
Zymomonas mobilis	[43]	Mn^{2+}	Competitive	40	600	ND[d]
Francisella tularensis	[84]	Mg^{2+}	STB assumed[e]	22	99	IC_{50} = 12.1 μM
Thermotoga maritima	[85]	Mg^{2+}	STB assumed[e]	50 85	16[g] 38[g]	ND[d]
Protozoa						
Plasmodium falciparum (native)	[94,118,119][h]		ND[d]			IC_{50} = 0.290–1.17 μM
Plasmodium falciparum (His-tagged)	[86]	Mn^{2+}	STB assumed[e]	30	21	ND[d]
Toxoplasma gondii (native)	[120]		ND[d]			No effect on culture
Toxoplasma gondii (His-tagged)	[41]	Mg^{2+}	STB assumed[e]	30	90	ND[d]
Plantae						
Arabidopsis thaliana	[39]	Mg^{2+}	Competitive	37	85	ND[d]
Coleus forskohlii	[40]	Mn^{2+}	ND[d]	37	148[i]	$IC_{50} \sim 1$ mM

[a] All enzymes are His-tagged fusions unless stated otherwise.
[b] Inhibition versus DXP.
[c] Minimum inhibitory concentration unless stated otherwise.
[d] ND = not determined.
[e] STB = slow tight binding. The enzyme was pre-incubated with fosmidomycin for 5–10 min prior to addition of DXP.
[f] Calculated from reported IC_{50} value of 310 nM, using the Cheng-Prusoff equation with 50 μM DXP and $K_{m,DXP}$ = 47 μM, as measured by the authors.
[g] Calculated from reported IC_{50} values of 93 nM (50 °C) and 107 nM (85 °C), using the Cheng-Prusoff equation with 200 μM DXP and $K_{m,DXP}$ = 40 μM (50 °C) and 110 μM (85 °C), as measured by the authors.
[h] Values are strain dependent.
[i] Calculated from reported IC_{50} value of 450 nM, using the Cheng-Prusoff equation with 300 μM DXP and $K_{m,DXP}$ = 147 μM, as measured by the authors.

at the dimer interface. As previously reported, the number of salt bridges varies for different species: three, eight, four, and fourteen for *E. coli*, *M. tuberculosis*, *Z. mobilis*, and *T. maritima* DXRs, respectively [85]. The large number in *T. maritima* DXR is believed to account for its thermostability. Sequence alignment of the structures of DXR from organisms listed in Tables 2 and 3 show high conservation of the residues from the catalytic domain (Fig. 10A, chain B) and variation of the peripheral domain residues, with an overall sequence identity fluctuating around 40%. Numerous publications provide multiple-sequence alignment of DXRs from various organisms, and the reader is referred to those sources [39,40,91,104,105].

5.2. Inhibitor–enzyme contacts

The active-site architecture of DXR with bound Mn^{2+}, NADPH, and inhibitor features three major nodes of interaction between the inhibitor and active-site residues: a metal-binding site, a phosphate-binding pocket, and flexible loop forming the lid over the active site (Fig. 10B). Interestingly, the binding mode of fosmidomycin was first interpreted as reflecting that of the intermediate MEsP, due to the presence of formyl groups in each [66]; however, it was later noted that based on the observed metal coordination of fosmidomycin's carbonyl, superposition of MEsP would predict the incorrect stereochemistry for hydride transfer [67]. Further, FR-900098, which bears an acetyl group in place of the formyl group of fosmidomycin and is therefore considered a closer mimic of DXP (Fig. 9A), was found to bind identically to fosmidomycin in quaternary complex with *M. tuberculosis* DXR, Mn^{2+}, and NADPH [104]. Fig. 10C schematically outlines the major interactions between functional groups of FR-900098 (or analogous functional groups of fosmidomycin) and DXR active site residues as observed in the crystal structures of *M. tuberculosis* [67,104], *E. coli* [66], and *P. falciparum* [78] DXRs.

Two oxygens of the hydroxamic head of the antibiotic coordinate to the divalent metal (Mn^{2+} in the case of *M. tuberculosis* and *E. coli* DXRs and Mg^{2+} for *P. falciparum* DXR) along with carboxylate groups of two glutamates and an aspartate. The coordination state of the metal cation was described as pentacoordinate with either trigonal bipyramidal geometry for the *P. falciparum* enzyme [78] or an approximately octahedral geometry for the *M. tuberculosis* enzyme [104]. Interestingly, for *E. coli* DXR a sixth coordination position of the metal cation (either Mn^{2+} or Mg^{2+}) was occupied by a water molecule, thus leading to a regular octahedral geometry [66,106]. In the absence of the inhibitor in the active site, the coordination status of metal cofactor is octahedral, with three water molecules and three carboxylate side chains occupying the coordination positions, as reported for *E. coli* [66], *M. tuberculosis* [67], and *T. maritima* [85] DXRs. Mutagenesis studies revealed the loss of metal binding and activity upon mutation of two of the three carboxylate residues to their uncharged amide analogues, as demonstrated for the *M. tuberculosis* DXR double mutant D151N/E222Q [67]. While the double mutant could still bind NADPH, fosmidomycin, and sulfate, these ligands exhibited increased dynamics, suggesting the loss of native conformation of the enzyme. Upon introduction of a single mutation in the metal-binding site of *Synechocystis* DXR, it was found

that loss of the aspartate charge is less detrimental than loss of the charge belonging to one of the glutamates, presumably involved in hydrogen-bonding interactions with the substrate [107]. Additionally, mutations of one of the glutamate residues for both *Synechocystis* [107] and *E. coli* [36] DXRs were rather detrimental to the catalysis than to the binding of the substrates. The influence of these and other mutations on the kinetic parameters of DXR is summarized in Table 4.

In addition to metal chelation, anchoring of the hydroxamic group of the inhibitor is believed to occur through hydrogen bonding to Ser152 (*M. tuberculosis*) [67] and Ser151 (*E. coli*) [37]. The effect of mutation of this conserved serine residue was probed for *Syhechocystis* DXR [107]; because S153N and S153T retained substantially more activity than S153A, it appears a residue capable of hydrogen bonding is required.

The phosphate-binding pocket of the DXR active is composed of a series of highly conserved amino acid residues forming multiple interactions with the phosphonate dianion of the inhibitor and similar interactions with the phosphate dianion of the substrate [37]. As shown in Fig. 10C, some of these interactions are conserved for DXRs from various species, while others have been observed only for DXRs from certain organisms (see figure caption for more details). Hydrogen-bond donors in the phosphate-binding pocket include an asparagine residue, two serine residues, and a lysine residue. Attempts to introduce an additional negative charge into the phosphate-binding pocket of *F. tularensis* DXR by mutation of one of the serine residues to glutamate or aspartate resulted in complete loss of activity [84].

5.3. DXR conformations

A variety of conformations have been captured in the crystal structures of various complexes of DXR, suggesting high conformational flexibility and dynamics of the enzyme. Molecular dynamics studies sampled multiple conformations of DXR, underscoring its flexibility [103]. For this reason solution NMR studies of DXR have been significantly compromised [101]. Most importantly, while the overall conformation of DXR domains remained essentially the same in complexes of DXR from various organisms, a conserved loop consisting of residues 198–206 (*M. tuberculosis* DXR), 291–299 (*P. falciparum* DXR), or 207–215 (*E. coli* DXR) was observed to adopt multiple conformations depending on the nature of the ligands bound in the active site. These conformations specifically involve various degrees of closure of the flexible loop over the active site, serving as a lid that shields the contents of active site from the bulk solvent. Additionally, closure of the flexible loop is often accompanied by movement of N- and C-terminal domains as rigid bodies towards each other and forming the active-site cleft. Two classifications of DXR conformations can be found in literature. The classification introduced in the work of Henriksson and co-workers [67] to categorize existing conformations of *E. coli* and *M. tuberculosis* DXR complexes is based on the distance across the active-site cleft, between residues 36 and 348 (*E. coli* DXR) and 47 and 339 of (*M. tuberculosis* DXR). According to this classification, crystal structures of *E. coli* DXR have been grouped into closed (17.6–18.4 Å), open (24.7–25.9 Å), and super-open (28 Å) forms (Fig. 11), while structures of *M. tuberculosis* DXR exhibit less

Table 4
Influence of active-site mutations on kinetic parameters of DXR.

Organism (reference)	Mutant	$(K_m)_{mut}/(K_m)_{WT}$		$\frac{(k_{cat})_{mut}}{(k_{cat})_{WT}}$	$\frac{(k_{cat}/K_{m,DXP})_{mut}}{(k_{cat}/K_{m,DXP})_{WT}}$
		DXP	NADPH		
Metal-binding-site residues					
M. tuberculosis [67]	D151N/E222Q		Inactive		
E. coli [36]	E231K	1.1	2.4	0.24%	0.22%
Synechocystis sp. [107]	D151A[a]		Inactive		
	D152N	7.1	2.3	2.4%	0.3%
	E154D[b]	1.2	1.5	0.3%	0.4%
	E154Q	0.008% activity of WT at 10 mM DXP			
	E223H[c]	0.007% activity of WT at 10 mM DXP			
	E223Q	Inactive			
Hydroxamic-binding residues					
Synechocystis sp. [107]	S153A[d]	8.1	2.5	0.1%	0.014%
	S153N	1.1	1.6	0.8%	0.6%
	S153T	8.6	4.9	4.8%	0.6%
Phosphate-binding-pocket residues					
F. tularensis [84]	S177E[e]	Inactive			
	S177D	Inactive			
Flexible-loop residues					
E. coli [36]	H209Q	7.6	2.4	0.15%	0.02%
Synechocystis sp. [107,109]	W204F[f]	2.5	1.0	59%	24%
	W204L	17.1	6.9	1.5%	0.09%
	W204V	29.4	ND	3.2%	0.11%
	W204A	70.6	ND	0.94%	0.013%
	M206A[g]	25.2	5.1	9.4%	0.4%
	M206V	Inactive			
M. tuberculosis [110]	W203F[f]	8.0	ND	38%	4.7%
	W203Y	2.8	ND	84%	29%
	W203A	Inactive			
	W203G	Inactive			

[a] Equivalent to D151 of *Ec*DXR.
[b] Equivalent to D153 of *Ec*DXR.
[c] Equivalent to E231 of *Ec*DXR.
[d] Equivalent to S151 of *Ec*DXR.
[e] Equivalent to S186 of *Ec*DXR.
[f] Equivalent to W212 of *Ec*DXR.
[g] Equivalent to M214 of *Ec*DXR.

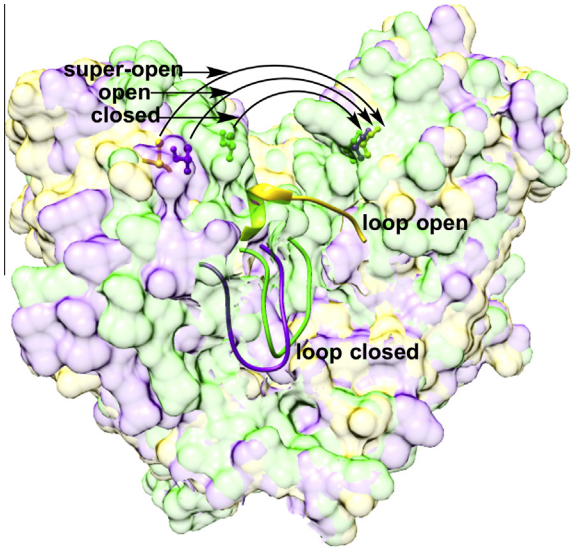

Fig. 11. Illustration of super-open (1K5H [122], chain A, gold), open (1T1S [123], chain B, purple) and closed (1Q0L [37], chain A, green) domain conformations, and open (1K5H) and closed (1T1S, 1Q0L) loop conformations of *E. coli* DXR. The image was created with UCSF Chimera [121].

variation of the cleft distances, falling in the range between open and closed conformations (20.3–25.0 Å). Another classification, described in the work of Takenoya and co-workers [85], is grouping the structures of *E. coli*, *M. tuberculosis*, *Z. mobilis* and *T. maritima* DXRs into four conformations, taking into account not only the size of the active-site cleft (adopting only two major forms in this classification: open domain and closed domain) but also the position of the flexible loop over the active site (open or closed). As observed in crystal structures of DXRs from various organisms, the closure of the flexible loop appears to be triggered by interactions with the phosphodianion group of the inhibitor or even its minimal analogue, inorganic sulfate dianion [67,91,108]. Based on the analysis of a series of crystal structures, Takenoya and co-workers suggested that closure of the domains and the flexible loop could only be achieved upon co-crystallization of the antibiotic (fosmidomycin or FR-900098) with the enzyme [37,67,78,85,104]. The only exclusion from this pattern was seen for the fully closed quaternary complex involving *T. maritima* DXR, Mg^{2+}, NADPH, and fosmidomycin, obtained upon soaking the metal-bound enzyme crystals in a solution of the two other ligands [85]. In contrast, soaking of the apo-form of the enzyme in the inhibitor solution resulted in formation of the open-domain/closed-loop form [66,106], suggesting that movement of the domains in the apo-form of DXR is restrained by crystal contacts. Interestingly, this complex has been suggested to represent the initially formed, loose E·I complex associated with the slow, tight binding of the inhibitor (recall Section 4.1).

5.4. Flexible loop

As illustrated in the Fig. 10C, residues of the flexible loop interact with different parts of FR-900098. The highly conserved tryptophan residue of the loop forms hydrophobic interactions with the methyl group of the hydroxamic acid. It is noteworthy that this residue plays an important role in substrate discrimination by DXR. Mutagenesis studies by Fernandes and co-workers [109] showed that whereas wild-type *Synechocystis* DXR does not turnover the larger substrate analogue 1-methyl-DXP, its W204F mutant accepts it as a slow alternative substrate, presumably due to reduced steric hindrance. Attempts to substitute this tryptophan with non-aromatic amino acids (Leu, Val or Ala) led to the mutants strongly impaired in both binding and catalytic properties [109]. Similarly, Kholodar and co-workers [110] demonstrated a lack of activity for W203G and W203A mutants of *M. tuberculosis* DXR. Interestingly, however, phenylalanine and tyrosine substitutions were well accommodated (Table 4), underscoring the necessity for an aromatic residue. Furthermore, W203F and W203Y exhibited greatly diminished burst kinetics and larger primary ^2H KIEs on k_{cat} than the wild-type enzyme (recall Section 3.2), indicating that mutation had rendered chemical steps more rate limiting. Surprisingly, fosmidomycin was found to bind more tightly to these mutants by up to an order of magnitude, a result that was attributable to a large increase in binding enthalpy [110].

Another highly conserved loop residue, His209 (*E. coli* DXR), is involved in an interaction with the phosphonate moiety of the inhibitor. Hydrogen bonding and/or salt bridging between this histidine and the phosphodianion of the ligand was suggested to be a factor favoring pre-orientation of the ligand in the active site and playing an important role in loop closure [37,104]. The importance of His209 has been indicated from a mutagenesis study with *Ec*DXR, in which H209Q exhibited an 8-fold increase in DXP's K_m and a 700-fold decrease in k_{cat} [36].

Additionally, reports indicate that the highly conserved methionine residue in the flexible loop (not shown in Fig. 10C) forms hydrophobic interactions with the backbone of the inhibitor or the nicotinamide moiety of NADPH [78]. Mutation of this residue to alanine or valine was reported to significantly impair DXP binding and turnover [107].

5.5. The role of the substrate's phosphodianion group

Abundant structural and kinetic evidence indicates the necessity of phosphodianion–enzyme interactions for activity of DXR's ligands as substrates or inhibitors and driving the major conformational rearrangements: closure of the flexible loop over the active site and tightening of the active site cleft (Fig. 11). These factors suggest that the phosphodianion group of the ligand does not simply serve as an anchoring functionality but modulates the active-site architecture, potentially leading to altered catalytic properties

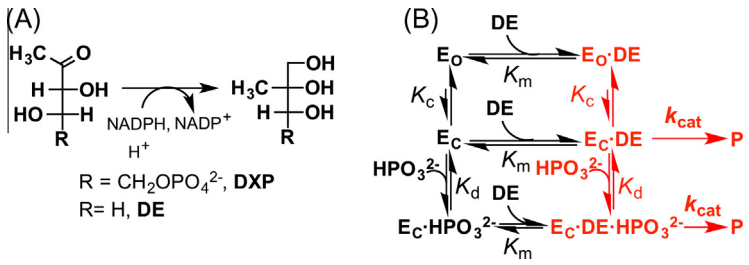

Fig. 12. (A) DXR-catalyzed reaction of natural substrate DXP and truncated substrate DE. (B) Kinetic scheme for rationalization of phosphite activation of the reaction of the "substrate in pieces" catalyzed by *M. tuberculosis* DXR.

of the enzyme. According to studies on the substrate specificity of *E. coli* DXR, the dephosphorylated version of DXP, 1-deoxy-D-xylulose, does not exhibit any measurable activity at the highest concentration (2 mM) used [29]. Curiously, the truncated substrate 1-deoxy-L-erythrulose, which lacks the terminal phosphorylmethyl group, can be turned over by *M. tuberculosis* DXR with a 3000-fold lower k_{cat} and 10^6-fold lower k_{cat}/K_m than the natural substrate DXP (Fig. 12A) [92]. The tremendous decrease of the second-order rate constant corresponds to a transition-state energy increase of 8.4 kcal/mol due to removal of by the non-reacting phosphorylmethyl group, assuming truncation does not alter the transition-state structure (this appears to be true for triosephosphate isomerase [111]). In the presence of inorganic phosphite dianion, the enzymatic function was partially complemented, resulting in an increase of first- and second-order rate constants by a factor of five. Thus, 3.2 kcal/mol of the lost transition-state stabilization was recovered in the reaction of "the substrate in pieces" [92]. These results agree with those of similar studies involving phosphite activation of reactions with truncated substrates for the mechanistically unrelated enzymes triosephosphate isomerase (TIM) [112], orotidine-5′-monophosphate decarboxylase (OMPDC) [113], and glycerol-3′-phosphate dehydrogenase (GPDH) [114]. DXR shares one common feature with these enzymes: a flexible loop that closes over the phosphate-binding pocket of the active site in the presence of phosphodianion or an analogue. The suggested general effect of this conformational change is to extrude water molecules from the active site, leading to a decrease in its effective dielectric constant [115]. This condition favors stronger interactions between active-site residues and transition states and/or intermediates of the reaction, which ultimately results in rate acceleration.

As illustrated by the kinetic scheme (Fig. 12B), the equilibrium between conformations of the free enzyme can be simplified to inactive loop-open (E_O) and active loop-closed (E_C) forms. While the truncated substrate can bind both conformations without influencing the equilibrium between them, phosphite dianion only binds to the loop-closed form, shifting the total conformational pool to the E_C form. Therefore, the central equilibrium between E_O and E_C (K_c) dictates the observed activation factor of truncated substrate turnover. Unlike TIM, OMPDC and GPDH, which exhibit significant activation factors ranging from $7 \cdot 10^2$ to $7 \cdot 10^4$, the modest fivefold activation observed for DXR indicates that more complexity is involved in the stabilization of its transitions state [92]. Most significantly, in contrast to these other enzymes, DXR employs a metal cofactor to position the substrate and stabilize the transitions state(s) and intermediate of the reaction. Therefore, the total binding energy of the rate-limiting transition state is split between the metal-chelating and phosphodianion termini of DXP, while the total binding energy of transition states for TIM, OMPDC, and GPDH is likely to be considerably concentrated on the phosphodianion functionality.

6. Conclusion

DXR has received thorough investigation over the past sixteen years due to its strong potential as a target for antibiotic and herbicide development and because of its intriguing rearrangement–reduction chemistry. Largely supported by studies employing substrate analogues and kinetic isotope effects, a retro-aldol/aldol mechanism is responsible for the isomerization of DXP to the aldehyde intermediate MEsP. Depending on the enzyme source and the degree of enzyme saturation, the retro-aldol, hydride-transfer, and MEP-release steps may limit DXP turnover to different extents. Fosmidomycin serves as a prototypical DXR inhibitor that has demonstrated high potency with the isolated enzyme but varied success in cell-based experiments. Knowledge of the chemical and kinetic mechanisms and of the nature of fosmidomycin binding and inhibition may drive the discovery of new DXR inhibitors with more favorable pharmaceutical properties.

Acknowledgments

This review was supported in part by a DuPont Young Professor award and a National Science Foundation CAREER award (CHE1255136) to A.S.M.

References

[1] J.W. Porter, S.L. Spurgeon, Biosynthesis of Isoprenoid Compounds, Wiley, New York, 1981.
[2] J.D. Connolly, R.A. Hill, Dictionary of Terpenoids, first ed., Chapman & Hall, London, New York, 1991.
[3] M. De Rosa, A. Gambacorta, A. Gliozzi, Microbiol. Rev. 50 (1986) 70–80.
[4] J.T. Mills, S.T. Furlong, E.A. Dawidowicz, Proc. Natl. Acad. Sci. USA 81 (1984) 1385–1388.
[5] J.C. Sacchettini, C.D. Poulter, Science 277 (1997) 1788–1789.
[6] S.O. Duke, F.E. Dayan, J.G. Romagni, A.M. Rimando, Weed Res. 40 (2000) 99–111.
[7] D.E. Cane, T. Rossi, J.P. Pachlatko, Tetrahedron Lett. (1979) 3639–3642.
[8] D.E. Cane, T. Rossi, A.M. Tillman, J.P. Pachlatko, J. Am. Chem. Soc. 103 (1981) 1838–1843.
[9] D. Zhou, R.H. White, Biochem. J. 273 (Pt 3) (1991) 627–634.
[10] S. Pandian, S. Saengchjan, T.S. Raman, Biochem. J. 196 (1981) 675–681.
[11] G. Flesch, M. Rohmer, Eur. J. Biochem. 175 (1988) 405–411.
[12] J. Schwender, M. Seemann, H.K. Lichtenthaler, M. Rohmer, Biochem. J. 316 (Pt 1) (1996) 73–80.
[13] H. Seto, H. Watanabe, K. Furihata, Tetrahedron Lett. 37 (1996) 7979–7982.
[14] H. Kleinig, Annu. Rev. Plant Physiol. Plant Mol. Biol. 40 (1989) 39–59.
[15] J. Chappell, Annu. Rev. Plant Physiol. Plant Mol. Biol. 46 (1995) 521–547.
[16] H.K. Lichtenthaler, M. Rohmer, J. Schwender, Physiol. Plant. 101 (1997) 643–652.
[17] T. Duvold, J.-M. Bravo, C. Pale-Grosdemange, M. Rohmer, Tetrahedron Lett. 38 (1997) 4769–4772.
[18] T. Duvold, P. Cali, J.-M. Bravo, M. Rohmer, Tetrahedron Lett. 38 (1997) 6181–6184.
[19] H.K. Lichtenthaler, J. Schwender, A. Disch, M. Rohmer, FEBS Lett. 400 (1997) 271–274.
[20] M. Rohmer, M. Knani, P. Simonin, B. Sutter, H. Sahm, Biochem. J. 295 (Pt 2) (1993) 517–524.
[21] M. Rohmer, M. Seemann, S. Horbach, S. Bringer-Meyer, H. Sahm, J. Am. Chem. Soc. 118 (1996) 2564–2566.
[22] L. Zhao, W.C. Chang, Y. Xiao, H.W. Liu, P. Liu, Annu. Rev. Biochem. 82 (2013) 497–530.
[23] T. Kuzuyama, T. Shimizu, S. Takahashi, H. Seto, Tetrahedron Lett. 39 (1998) 7913–7916.
[24] L.M. Lois, N. Campos, S.R. Putra, K. Danielsen, M. Rohmer, A. Boronat, Proc. Natl. Acad. Sci. USA 95 (1998) 2105–2110.
[25] J. Schwender, J. Zeidler, R. Groner, C. Muller, M. Focke, S. Braun, F.W. Lichtenthaler, H.K. Lichtenthaler, FEBS Lett. 414 (1997) 129–134.
[26] N. Singh, G. Cheve, M.A. Avery, C.R. McCurdy, Curr. Pharm. Des. 13 (2007) 1161–1177.
[27] J. Querol, N. Campos, S. Imperial, A. Boronat, M. Rodriguez-Concepcion, FEBS Lett. 514 (2002) 343–346.
[28] B.M. Lange, T. Rujan, W. Martin, R. Croteau, Proc. Natl. Acad. Sci. USA 97 (2000) 13172–13177.
[29] S. Takahashi, T. Kuzuyama, H. Watanabe, H. Seto, Proc. Natl. Acad. Sci. USA 95 (1998) 9879–9884.
[30] M. Rodriguez-Concepcion, N. Campos, L. Maria Lois, C. Maldonado, J.F. Hoeffler, C. Grosdemange-Billiard, M. Rohmer, A. Boronat, FEBS Lett. 473 (2000) 328–332.
[31] J. Schwender, C. Muller, J. Zeidler, H.K. Lichtenthaler, FEBS Lett. 455 (1999) 140–144.
[32] K. Kobayashi, S.D. Ehrlich, A. Albertini, G. Amati, K.K. Andersen, M. Arnaud, K. Asai, S. Ashikaga, S. Aymerich, P. Bessieres, et al., Proc. Natl. Acad. Sci. USA 100 (2003) 4678–4683.
[33] A. Argyrou, J.S. Blanchard, Biochemistry 43 (2004) 4375–4384.
[34] X. Yin, P.J. Proteau, Biochim. Biophys. Acta 1652 (2003) 75–81.
[35] A.T. Koppisch, D.T. Fox, B.S. Blagg, C.D. Poulter, Biochemistry 41 (2002) 236–243.
[36] T. Kuzuyama, S. Takahashi, M. Takagi, H. Seto, J. Biol. Chem. 275 (2000) 19928–19932.
[37] A. Mac Sweeney, R. Lange, R.P. Fernandes, H. Schulz, G.E. Dale, A. Douangamath, P.J. Proteau, C. Oefner, J. Mol. Biol. 345 (2005) 115–127.
[38] R. Crichton, Biological Inorganic Chemistry: A New Introduction to Molecular Structure and Function, second ed., Elsevier Science & Technology, Amsterdam, NLD, 2012.
[39] F. Rohdich, S. Lauw, J. Kaiser, R. Feicht, P. Kohler, A. Bacher, W. Eisenreich, FEBS J. 273 (2006) 4446–4458.

[40] S. Engprasert, F. Taura, Y. Shoyama, Plant Sci. (Amsterdam, Neth.) 169 (2005) 287–294.
[41] G. Cai, L. Deng, J. Xue, S.N. Moreno, B. Striepen, Y. Song, Bioorg. Med. Chem. Lett. 23 (2013) 2158–2161.
[42] B. Miller, T. Heuser, W. Zimmer, FEBS Lett. 481 (2000) 221–226.
[43] S. Grolle, S. Bringer-Meyer, H. Sahm, FEMS Microbiol. Lett. 191 (2000) 131–137.
[44] P.J. Proteau, Y.H. Woo, R.T. Williamson, C. Phaosiri, Org. Lett. 1 (1999) 921–923.
[45] D. Arigoni, W. Eisenreich, C. Latzel, S. Sagner, T. Radykewicz, M.H. Zenk, A. Bacher, Proc. Natl. Acad. Sci. USA 96 (1999) 1309–1314.
[46] T. Radykewicz, F. Rohdich, J. Wungsintaweekul, S. Herz, K. Kis, W. Eisenreich, A. Bacher, M.H. Zenk, D. Arigoni, FEBS Lett. 465 (2000) 157–160.
[47] D. Arigoni, J.-L. Giner, S. Sagner, J.H. Wungsintaweekul, M. Zenk, K. Kis, A. Bacher, W. Eisenreich, Chem. Commun. (1999) 1127–1128.
[48] D. Arigoni, S. Sagner, C. Latzel, W. Eisenreich, A. Bacher, M.H. Zenk, Proc. Natl. Acad. Sci. USA 94 (1997) 10600–10605.
[49] S.R. Putra, L.M. Lois, N. Campos, A. Boronat, M. Rohmer, Tetrahedron Lett. 39 (1998) 23–26.
[50] H.E. Umbarger, B. Brown, E.J. Eyring, J. Biol. Chem. 235 (1960) 1425–1432.
[51] K. Kiritani, S. Narise, R.P. Wagner, J. Biol. Chem. 241 (1966) 2042–2046.
[52] S.M. Arfin, H.E. Umbarger, J. Biol. Chem. 244 (1969) 1118–1127.
[53] R. Dumas, V. Biou, F. Halgand, R. Douce, R.G. Duggleby, Acc. Chem. Res. 34 (2001) 399–408.
[54] J.F. Hoeffler, D. Tritsch, C. Grosdemange-Billiard, M. Rohmer, Eur. J. Biochem. 269 (2002) 4446–4457.
[55] S.K. Chunduru, G.T. Mrachko, K.C. Calvo, Biochemistry 28 (1989) 486–493.
[56] D.B. Northrop, J. Chem. Educ. 75 (1998) 1153–1157.
[57] R. Dumas, D. Job, J.Y. Ortholand, G. Emeric, A. Greiner, R. Douce, Biochem. J. 288 (Pt 3) (1992) 865–874.
[58] D.E. Koshland Jr., K.E. Neet, Annu. Rev. Biochem. 37 (1968) 359–410.
[59] S. Hecht, J. Wungsintaweekul, F. Rohdich, K. Kis, T. Radykewicz, C.A. Schuhr, W. Eisenreich, G. Richter, A. Bacher, J. Org. Chem. 66 (2001) 7770–7775.
[60] A.E. Johnson, M.E. Tanner, Biochemistry 37 (1998) 5746–5754.
[61] L.V. Lee, M.V. Vu, W.W. Cleland, Biochemistry 39 (2000) 4808–4820.
[62] D.T. Fox, C.D. Poulter, Biochemistry 44 (2005) 8360–8368.
[63] S. Lauw, V. Illarionova, A. Bacher, F. Rohdich, W. Eisenreich, FEBS J. 275 (2008) 4060–4073.
[64] H. Li, J. Tian, W. Sun, W. Qin, W.Y. Gao, FEBS J. 280 (2013) 5896–5905.
[65] A. Wong, J.W. Munos, V. Devasthali, K.A. Johnson, H.W. Liu, Org. Lett. 6 (2004) 3625–3628.
[66] S. Steinbacher, J. Kaiser, W. Eisenreich, R. Huber, A. Bacher, F. Rohdich, J. Biol. Chem. 278 (2003) 18401–18407.
[67] L.M. Henriksson, T. Unge, J. Carlsson, J. Aqvist, S.L. Mowbray, T.A. Jones, J. Biol. Chem. 282 (2007) 19905–19916.
[68] C. Phaosiri, P.J. Proteau, Bioorg. Med. Chem. Lett. 14 (2004) 5309–5312.
[69] G.C. Levy, J.D. Cargioli, W. Racela, J. Am. Chem. Soc. 92 (1970) 6238–6246.
[70] J.W. Munos, X. Pu, S.O. Mansoorabadi, H.J. Kim, H.W. Liu, J. Am. Chem. Soc. 131 (2009) 2048–2049.
[71] U. Wong, R.J. Cox, Angew. Chem., Int. Ed. 46 (2007) 4926–4929.
[72] R.J. Cox, A. de Andres-Gomez, C.R. Godfrey, Org. Biomol. Chem. 1 (2003) 3173–3177.
[73] M.I. Schimerlik, J.E. Rife, W.W. Cleland, Biochemistry 14 (1975) 5347–5354.
[74] K.A. Manning, B. Sathyamoorthy, A. Eletsky, T. Szyperski, A.S. Murkin, J. Am. Chem. Soc. 134 (2012) 20589–20592.
[75] J. Liu, A.S. Murkin, Biochemistry 51 (2012) 5307–5319.
[76] J. Stackhouse, K.P. Nambiar, J.J. Burbaum, D.M. Stauffer, S.A. Benner, J. Am. Chem. Soc. 107 (1985) 2757–2763.
[77] M. Okuhara, Y. Kuroda, T. Goto, M. Okamoto, H. Terano, M. Kohsaka, H. Aoki, H. Imanaka, J. Antibiot. (Tokyo) 33 (1980) 24–28.
[78] T. Umeda, N. Tanaka, Y. Kusakabe, M. Nakanishi, Y. Kitade, K.T. Nakamura, Sci. Rep. 1 (2011) 9.
[79] E. Uh, E.R. Jackson, G. San Jose, M. Maddox, R.E. Lee, R.E. Lee, H.I. Boshoff, C.S. Dowd, Bioorg. Med. Chem. Lett. 21 (2011) 6973–6976.
[80] Y.H. Woo, R.P. Fernandes, P.J. Proteau, Bioorg. Med. Chem. 14 (2006) 2375–2385.
[81] L. Kuntz, D. Tritsch, C. Grosdemange-Billiard, A. Hemmerlin, A. Willem, T.J. Bach, M. Rohmer, Biochem. J. 386 (2005) 127–135.
[82] J.F. Morrison, C.T. Walsh, Adv. Enzymol. Ramb. 61 (1988) 201–301.
[83] L. Mercklé, A. de Andres-Gomez, B. Dick, R.J. Cox, C.R. Godfrey, ChemBioChem 6 (2005) 1866–1874.
[84] S. Jawaid, H. Seidle, W. Zhou, H. Abdirahman, M. Abadeer, J.H. Hix, M.L. van Hoek, R.D. Couch, PLoS One 4 (2009) e8288.
[85] M. Takenoya, A. Ohtaki, K. Noguchi, K. Endo, Y. Sasaki, K. Ohsawa, S. Yajima, M. Yohda, J. Struct. Biol. 170 (2010) 532–539.
[86] G. Cai, L. Deng, B.G. Fryszczyn, N.G. Brown, Z. Liu, H. Jiang, T. Palzkill, Y. Song, ACS Med. Chem. Lett. 3 (2012) 496–500.
[87] L. Deng, K. Endo, M. Kato, G. Cheng, S. Yajima, Y. Song, ACS Med. Chem. Lett. 2 (2011) 165–170.
[88] L. Deng, J. Diao, P. Chen, V. Pujari, Y. Yao, G. Cheng, D.C. Crick, B.V. Prasad, Y. Song, J. Med. Chem. 54 (2011) 4721–4734.
[89] J. Perruchon, R. Ortmann, M. Altenkamper, K. Silber, J. Wiesner, H. Jomaa, G. Klebe, M. Schlitzer, ChemMedChem 3 (2008) 1232–1241.
[90] C. Zingle, L. Kuntz, D. Tritsch, C. Grosdemange-Billiard, M. Rohmer, J. Org. Chem. 75 (2010) 3203–3207.
[91] L.M. Henriksson, C. Bjorkelid, S.L. Mowbray, T. Unge, Acta Crystallogr. D: Biol. Crystallogr. 62 (2006) 807–813.
[92] S.A. Kholodar, A.S. Murkin, Biochemistry 52 (2013) 2302–2308.
[93] A. Kunfermann, C. Lienau, B. Illarionov, J. Held, T. Grawert, C.T. Behrendt, P. Werner, S. Hahn, W. Eisenreich, U. Riederer, et al., J. Med. Chem. 56 (2013) 8151–8162.
[94] H. Jomaa, J. Wiesner, S. Sanderbrand, B. Altincicek, C. Weidemeyer, M. Hintz, I. Turbachova, M. Eberl, J. Zeidler, H.K. Lichtenthaler, et al., Science 285 (1999) 1573–1576.
[95] S. Borrmann, I. Lundgren, S. Oyakhirome, B. Impouma, P.B. Matsiegui, A.A. Adegnika, S. Issifou, J.F. Kun, D. Hutchinson, J. Wiesner, et al., Antimicrob. Agents Chemother. 50 (2006) 2713–2718.
[96] R.K. Dhiman, M.L. Schaeffer, A.M. Bailey, C.A. Testa, H. Scherman, D.C. Crick, J. Bacteriol. 187 (2005) 8395–8402.
[97] A.C. Brown, T. Parish, BMC Microbiol. 8 (2008) 78.
[98] K. Brucher, B. Illarionov, J. Held, S. Tschan, A. Kunfermann, M.K. Pein, A. Bacher, T. Grawert, L. Maes, B. Mordmuller, et al., J. Med. Chem. 55 (2012) 6566–6575.
[99] V. Devreux, J. Wiesner, J.L. Goeman, J. Van der Eycken, H. Jomaa, S. Van Calenbergh, J. Med. Chem. 49 (2006) 2656–2660.
[100] A.T. Nguyen-Trung, D. Tritsch, C. Grosdemange-Billiard, M. Rohmer, Bioorg. Med. Chem. Lett. 23 (2013) 1643–1647.
[101] N.E. Englert, C. Richter, J. Wiesner, M. Hintz, H. Jomaa, H. Schwalbe, ChemBioChem 12 (2011) 468–476.
[102] M. Pellecchia, D. Meininger, Q. Dong, E. Chang, R. Jack, D.S. Sem, J. Biomol. NMR 22 (2002) 165–173.
[103] S.L. Williams, J. Andrew McCammon, Chem. Biol. Drug Des. 73 (2009) 26–38.
[104] C. Bjorkelid, T. Bergfors, T. Unge, S.L. Mowbray, T.A. Jones, Acta Crystallogr. D: Biol. Crystallogr. 68 (2012) 134–143.
[105] S. Ricagno, S. Grolle, S. Bringer-Meyer, H. Sahm, Y. Lindqvist, G. Schneider, Biochim. Biophys. Acta 1698 (2004) 37–44.
[106] S. Yajima, K. Hara, D. Iino, Y. Sasaki, T. Kuzuyama, K. Ohsawa, H. Seto, Acta Crystallogr., Sect. F: Struct. Biol. Cryst. Commun. 63 (2007) 466–470.
[107] R.P. Fernandes, P.J. Proteau, Biochim. Biophys. Acta 1764 (2006) 223–229.
[108] S. Yajima, T. Nonaka, T. Kuzuyama, H. Seto, K. Ohsawa, J. Biochem. 131 (2002) 313–317.
[109] R.P. Fernandes, C. Phaosiri, P.J. Proteau, Arch. Biochem. Biophys. 444 (2005) 159–164.
[110] S.A. Kholodar, G. Tombline, J. Liu, Z. Tan, C.L. Allen, A.M. Gulick, A.S. Murkin, Biochemistry 53 (2014) 3423–3431.
[111] X. Zhai, T.L. Amyes, J.P. Richard, J. Am. Chem. Soc. (2014).
[112] J.P. Richard, Biochemistry 51 (2012) 2652–2661.
[113] T.L. Amyes, S.A. Ming, L.M. Goldman, B.M. Wood, B.J. Desai, J.A. Gerlt, J.P. Richard, Biochemistry 51 (2012) 4630–4632.
[114] W.Y. Tsang, T.L. Amyes, J.P. Richard, Biochemistry 47 (2008) 4575–4582.
[115] M.M. Malabanan, T.L. Amyes, J.P. Richard, Curr. Opin. Struct. Biol. 20 (2010) 702–710.
[116] O. Meyer, C. Grosdemange-Billiard, D. Tritsch, M. Rohmer, Org. Biomol. Chem. 1 (2003) 4367–4372.
[117] D.E. Cane, C. Chow, A. Lillo, I. Kang, Bioorg. Med. Chem. 9 (2001) 1467–1477.
[118] T. Verbrugghen, P. Vandurm, J. Pouyez, L. Maes, J. Wouters, S. Van Calenbergh, J. Med. Chem. 56 (2013) 376–380.
[119] J. Xue, J. Diao, G. Cai, L. Deng, B. Zheng, Y. Yao, Y. Song, ACS Med. Chem. Lett. 4 (2013) 278–282.
[120] S.C. Nair, C.F. Brooks, C.D. Goodman, A. Sturm, G.I. McFadden, S. Sundriyal, J.L. Anglin, Y. Song, S.N. Moreno, B. Striepen, J. Exp. Med. 208 (2011) 1547–1559.
[121] E.F. Pettersen, T.D. Goddard, C.C. Huang, G.S. Couch, D.M. Greenblatt, E.C. Meng, T.E. Ferrin, J. Comput. Chem. 25 (2004) 1605–1612.
[122] K. Reuter, S. Sanderbrand, H. Jomaa, J. Wiesner, I. Steinbrecher, E. Beck, M. Hintz, G. Klebe, M.T. Stubbs, J. Biol. Chem. 277 (2002) 5378–5384.
[123] S. Yajima, K. Hara, J.M. Sanders, F. Yin, K. Ohsawa, J. Wiesner, H. Jomaa, E. Oldfield, J. Am. Chem. Soc. 126 (2004) 10824–10825.